Atmos. Chem. Phys. Discuss., doi:10.5194/acp-2016-958, 2016
Manuscript under review for journal Atmos. Chem. Phys.
Published: 28 November 2016

Atmospheric Chemistry and Physics Discussions

Impact of Intercontinental Pollution Transport on North American Ozone Air Pollution: An HTAP Phase II Multi-model Study

Min Huang[1,2], Gregory R. Carmichael[3], R. Bradley Pierce[4], Duseong S. Jo[5], Rokjin J. Park[5], Johannes Flemming[6], Louisa K. Emmons[7], Kevin W. Bowman[8], Daven K. Henze[9], Yanko Davila[9], Kengo Sudo[10], Jan Eiof Jonson[11], Marianne Tronstad Lund[12], Greet Janssens-Maenhout[13], Frank J. Dentener[13], Terry J. Keating[14], Hilke Oetjen[8,*], Vivienne H. Payne[8]

[1]George Mason University, Fairfax, VA, USA
[2]University of Maryland, College Park, MD, USA
[3]University of Iowa, Iowa City, IA, USA
[4]NOAA National Environmental Satellite, Data, and Information Service, Madison, WI, USA
[5]Seoul National University, Seoul, Korea
[6]European Center for Medium range Weather Forecasting, Reading, UK
[7]National Center for Atmospheric Research, Boulder, CO, USA
[8]Jet Propulsion Laboratory, California Institute of Technology, Pasadena, CA, USA
[9]University of Colorado-Boulder, Boulder, CO, USA
[10]Nagoya University, Furocho, Chigusa-ku, Nagoya, Japan
[11]Norwegian Meteorological Institute, Oslo, Norway
[12]Center for International Climate and Environmental Research, Oslo, Norway
[13]European Commission, Joint Research Center, Ispra, Italy
[14]US Environmental Protection Agency, Research Triangle Park, NC, USA
[*]Now at: University of Leicester, Leicester, UK

Correspondence to: Min Huang (mhuang10@gmu.edu)

Abstract

The recent update on the US National Ambient Air Quality Standards of the ground-level ozone (O_3) can benefit from a better understanding of its source contributions in different US regions during recent years. In the Hemispheric Transport of Air Pollution experiment Phase 1 (HTAP1), various global models were used to determine the O_3 source-receptor relationships among three continents in the North Hemisphere in 2001. In support of the HTAP Phase 2 (HTAP2) experiment that studies more recent years and involves higher-resolution global models and regional models' participation, we conduct a number of regional scale Sulfur Transport and dEposition Model (STEM) air quality base and sensitivity simulations over North America during May-June 2010. The STEM top and lateral chemical boundary conditions were downscaled from three global chemical transport models' (i.e., GEOS-Chem, RAQMS, and ECMWF C-IFS) base and sensitivity simulations (in which the East Asian anthropogenic emissions were reduced by 20%). We perform analyses not only on large spatial/temporal scales relative to the HTAP1, but also on subcontinental- and event-scale that are more relevant to the US air quality management. The differences between STEM surface O_3 sensitivities (including the 24h mean and the US policy-relevant maximum daily 8h average (MDA8) metric averaged throughout the study period and during a selected pollution transport event) and its corresponding boundary condition model's are often smaller than those among its boundary condition models. The STEM sensitivities are also compared with the mean sensitivities estimated by multi- global models, which are higher

Atmos. Chem. Phys. Discuss., doi:10.5194/acp-2016-958, 2016
Manuscript under review for journal Atmos. Chem. Phys.
Published: 28 November 2016

Atmospheric Chemistry and Physics Discussions

than the HTAP1 reported 2001 conditions, as well as the 2001-2005 conditions studied using the tagged tracer approach. This indicates the increasing impacts of the East Asian anthropogenic pollution on North America during 2001-2010. The GEOS-Chem sensitivities indicate that the East Asian anthropogenic NO_x emissions matter more than the other East Asian O_3 precursors to the North American O_3, qualitatively consistent with previous adjoint sensitivity calculations. An additional STEM simulation was performed in which the boundary conditions were downscaled from a global RAQMS simulation without East Asian anthropogenic emissions, to assess the scalability of O_3 sensitivities to the size of the emission perturbation. The scalability is spatially varying, and the full source contribution obtained by linearly scaling the North American regional mean O_3 sensitivity to the 20% reduction in the East Asian emissions may be underestimated.

Satellite NO_2 (KNMI OMI) and O_3 (TES, JPL-IASI, OMI, MLS, and AIRS) products help detect pollution episodes, quantify or/and reduce the uncertainties in the bottom-up NO_x emissions and the model transported background O_3. Based on model calculations and satellite/surface observations during a selected event, we show the different influences from stratospheric O_3 intrusions along with the transported East Asian pollution on O_3 in the western and the eastern US. Future directions of using satellite data in air quality research are also suggested.

1. Introduction

Tropospheric ozone (O_3), a short-lived trace gas with a lifetime ranging from hours in the boundary layer to weeks in the free troposphere, affects tropospheric chemistry, harms human and ecosystem health, and induces climate change on local, regional and global scales (Jerrett et al., 2009; Smith et al., 2009; Anenberg et al., 2010; Mauzerall and Wang, 2001; Avnery et al., 2011a, b; Shindell et al., 2009, 2013; Bowman and Henze, 2012; Stevenson et al., 2006, 2013; Monks et al., 2015). It has been recognized that the uneven distributions of tropospheric O_3 can be attributed to the stratosphere as well as local, regional and distant emission sources, through complicated processes that occur on synoptic, meso- and micro-scales (Task Force on Hemispheric Transport of Air Pollution (HTAP), 2010; National Research Council (NRC), 2009; Maas and Grennfelt, 2016). The mitigation of O_3's climate and health impacts would benefit from efforts to control the emissions of its precursors from the various emission sources (United Nations Environment Programme (UNEP) and World Meteorological Organization (WMO), 2011), such as nitrogen oxides (NO_x), carbon monoxide (CO), methane (CH_4), and non-methane volatile organic compounds (NMVOCs).

Ground-level O_3 is one of the six criteria air pollutants regulated by the US Environmental Protection Agency (EPA), and the US National Ambient Air Quality Standards (NAAQS) has recently been lowered to 70 ppbv to better protect Americans' health and the environment. Issues regarding making accurate estimates of the total O_3 as well as the background O_3 level (defined as the concentration that is not affected by recent locally-emitted or produced anthropogenic pollution) (e.g., McDonald-Buller et al., 2011; Zhang et al., 2011; Fiore et al., 2014; Huang et al., 2015), have been recently discussed as part of the implementation of the new US O_3 standard (US EPA, 2016a, b). This includes assessing the impacts of various components of the background O_3, such as stratospheric O_3, local natural sources such as biogenic, lightning and wildfire emissions, as well as the long-range transport (LRT) of pollution. The impact of the trans-Pacific pollution transport on US air quality has been evaluated in numerous studies over the past decades (e.g., Fiore et al., 2009; Reidmiller et al., 2009; Zhang et al., 2008, 2009; Huang et al., 2010, 2013a; Lin

Atmos. Chem. Phys. Discuss., doi:10.5194/acp-2016-958, 2016
Manuscript under review for journal Atmos. Chem. Phys.
Published: 28 November 2016

Atmospheric Chemistry and Physics Discussions

et al., 2012a; US EPA, 2016a). It has been found that the increasing trends of pollution in the upwind continents, especially the populated East Asia (e.g., Zhang et al., 2014; Susaya et al., 2013; Wang et al., 2012), may partially offset the US air quality improvements in recent decades due to the regional and local emission controls (e.g., Verstraeten et al., 2015; Ambrose et al., 2011; Wigder et al., 2013; Cooper et al., 2010; Parrish et al., 2009, 2012; Gratz et al., 2014). A better understanding of the processes that determine the O_3 pollution levels, as well as an improved capability of attributing the air pollution to nearby or distant sources is needed to assist with designing and implementing effective local emission control strategies to comply with the tighter air quality standards.

Chemical transport models are often used to reproduce and attribute the observed O_3 levels, including assessing the impacts of the internationally transported O_3 on the US air quality. In the HTAP modeling experiment Phase I (HTAP1), various global models with horizontal resolutions ranging from 1°×1° to 5°×5°, only around half of which are finer than 3°×3°, were used to determine the O_3 source-receptor (SR) relationships among three continents in the Northern Hemisphere in 2001 (Chapter 4 in HTAP, 2010). The global model based SR relationships in HTAP1 determined using the emission perturbation approach (i.e., calculating the changes of O_3 at the receptor regions in response to a 20% reduction in the emission inputs in a given source region) were reported as either monthly 24h mean values or policy-relevant metrics such as the maximum daily 8h average (MDA8) for the US (e.g., Fiore et al., 2009; Reidmiller et al., 2009). Large intermodel diversity was found in the simulated total O_3 and the intercontinentally transported pollution for the chosen SR pairs in the northern midlatitudes, indicating the challenges with model simulations to accurately represent the key atmospheric processes. Multi-model mean results were the foci of in these studies with the assumption that this approach can reduce the uncertainty from the single model estimates for monthly or seasonal means. “Ensemble” model analyses have been suggested by some US stakeholders as one of the methods for helping with the characterization of the background O_3 components (US EPA, 2016b). Although the multi-model approach can help identify some of the weaknesses of the individual models and may produce more reliable estimates, it is necessary to well understand the uncertainties inherent in using the same set of anthropogenic emissions in all these model simulations. Satellite observations over the regions with limited in-situ measurements such as the East Asia can be particularly helpful for quantifying such uncertainties.

The 20% emission perturbation in the HTAP1 modeling experiment was chosen to produce a sizeable (i.e., larger than numerical noise) and realistic impact, but small enough in the assumed near-linear atmospheric chemistry regime. The scalability of the modeled O_3 sensitivities to the size of the emission perturbations has been assessed on continental scale (Wu et al., 2009; Fiore et al., 2009; HTAP, 2010; Wild et al., 2012; Emmons et al., 2012). The receptor O_3 responses to the source-region emission perturbations are found to be fairly linear within ~50% of the perturbations. However, due to the chemical non-linearity, the full source contribution obtained by linearly scaling the receptor regional mean O_3 sensitivity to the 20% reduction in the source region emissions may be underestimated, and the scalability depended on seasons and the perturbed emission species. Huang et al. (2013b) investigated the scalability of the O_3 sensitivity between the southern California-US intermountain west SR pair for May 2010, in which study the southern California anthropogenic emissions were perturbed by multiple amounts of +50%, -50%, -100%. They reported that the scalability of the O_3 sensitivities changed with the distance from the source

Atmos. Chem. Phys. Discuss., doi:10.5194/acp-2016-958, 2016
Manuscript under review for journal Atmos. Chem. Phys.
Published: 28 November 2016

Atmospheric Chemistry and Physics Discussions

regions. Further analyses on the scalability of these modeled O_3 sensitivities during recent years especially for the East Asia-NAM SR pair, as well as their spatial variability, are still needed. Furthermore, results generated using the emission perturbation approach need to be compared with those based on the other methods (e.g., tagged tracers, adjoint sensitivity).

Previous studies have demonstrated the advantages of high resolution chemical transport modeling for understanding SR relationships (e.g., Lin et al., 2010 for Europe and the East Asia; Lin et al., 2012a; Huang et al., 2010, 2013a for Asia and NAM). Using observations (satellite, sondes, aircraft) along with single model simulations, a few studies have reported that the US O_3 sensitivities to extra-regional sources is region-dependent (e.g., Lin et al., 2012a, b; Langford et al., 2011; Ott et al., 2016), and therefore the necessity of evaluating the extra-regional source impacts on event scale has been emphasized in these studies as well as in US EPA (2016a, b). The HTAP Phase 2 (HTAP2) multi-model experiment, initiated in 2012, is designed to advance the understanding of the impact of intercontinental pollution transport during more recent years (i.e., 2008-2010) involving a number of global and regional models' participation (Galmarini et al., 2016; Koffi et al., 2016). The regional models are anticipated to help connect the analyses over global and regional scales and enable discussions on small spatial (e.g., subcontinental) and temporal scales (i.e., event based analyses). The use of satellite products for identifying the transport events as well as for quantitative model evaluation is also encouraged in the work plan. The HTAP2 modeling experiment was sequentially conducted in two steps. First, similar to the HTAP1 experiment, a group of global models with different resolutions conducted base and emission perturbation sensitivity simulations to determine the pollutants' SR relationships. All models in their base simulations used the same set of harmonized sector-based global anthropogenic emissions developed specifically for the HTAP2 modeling experiment (Janssens-Maenhout et al., 2015). Most of these global models recorded only key chemical species from their base and sensitivity simulations in varied temporal frequencies. Several global models saved the three-dimensional (3D) chemical fields of more species with a 3- or 6-hour interval, which are suitable for being used as regional models' chemical boundary conditions. In the second step, regional models conducted base and sensitivity simulations to analyze the pollutants' SR relationships in greater detail. The regional model simulations used the same set of anthropogenic emissions as the global models within their simulation domains, and the chemical boundary conditions in these regional simulations were downscaled from the base and sensitivity simulations from the selected boundary condition model outputs. For regional simulations over the North America and Europe, boundary conditions were mostly taken from a single model such as the ECMWF C-IFS or GEOS-Chem.

In this study, we performed a number of regional scale STEM (Sulfur Transport and dEposition Model) base and sensitivity simulations over the NAM during May-June 2010, during which period strong trans-Pacific pollution transport were shown to episodically impact the US (Lin et al., 2012a). Extending the HTAP2 regional simulations' basic setup, the STEM top and lateral chemical boundary conditions were downscaled from three global models' (i.e., the Seoul National University (SNU) GEOS-Chem, RAQMS, and the ECMWF C-IFS) base and sensitivity simulations in which the East Asian anthropogenic emissions were reduced. The STEM surface O_3 sensitivities over the NAM region based on different boundary condition models were inter-compared, in terms of the regional averages and the spatial patterns on monthly basis and during a selected event identified by satellite O_3 and CO products. These were also compared with the

Atmos. Chem. Phys. Discuss., doi:10.5194/acp-2016-958, 2016
Manuscript under review for journal Atmos. Chem. Phys.
Published: 28 November 2016

Atmospheric Chemistry and Physics Discussions

sensitivities estimated by their corresponding boundary condition models as well as all HTAP2 participating global models. An additional regional simulation was performed in which the STEM boundary conditions were downscaled from one global model simulation without the East Asian anthropogenic emissions, and the nonlinear relationship between the O_3 sensitivity and the size of the emission perturbation is discussed. In the discussion, we emphasize: 1) the differences in O_3 sensitivities generated from the HTAP2 and HTAP1 experiments to help address how the LRT impacts on NAM changed through time; 2) how the multi-model approach, as well as the refined model experiment design in HTAP2 can help advance our understanding of the LRT impacts, especially the benefits of increasing the global models' resolutions and involving the regional models; 3) the usefulness of satellite observations for better understanding the sources of uncertainties in the modeled total O_3 (e.g., from the emission and regional models' boundary condition inputs) as well as for reducing the uncertainties in some of these model inputs via chemical data assimilation.

2. Methods

2.1. Anthropogenic emission inputs

Identical anthropogenic emissions were used in all global and regional chemical transport models' base and sensitivity simulations. This monthly-varying harmonized sectoral (i.e., power, industry, transportation, residential, shipping, aircraft, agriculture) emission inventory was provided on a gridded 0.1°×0.1° resolution for the years of 2008 and 2010, by compiling the officially reported emissions at the national scale (Janssens-Maenhout et al., 2015; http://edgar.jrc.ec.europa.eu/htap_v2). The temporal profiles for developing the monthly-varying emissions differ by region and sector. The amount of emissions of key O_3 precursors (CO, NO_x, NMVOCs) from both years are summarized in Table S1 for the four major emissions sectors, over the NAM (US+Canada, based on data from the US EPA and the Environmental Canada, which shows lower emissions from the previous years as also discussed in Pouliot et al., 2015), MICS-Asia regions (south, southeast, and east Asia, based on country inventory for China and from the Clean Air Policy Support System and the Regional Emission inventory in ASia 2.1, more information also in Li et al., 2015), and for over the world. For all of these species, global total emissions in 2008 and 2010 are similar. The NO_x, NMVOC, and CO emissions decreased from 2008 to 2010 over the NAM by 10.7%, 9.4%, and 15.7%, respectively. For 2010, the transportation sector contributed more than the other sectors to NAM anthropogenic NO_x and CO emissions; industrial sector contributed more than the other sectors to NMVOCs emissions. Over East Asian countries, these emissions are ~2-5 times higher than the US emissions, and the NO_x, NMVOC and CO emissions increased over Asia by 7.3%, 7.2% and 1.0%, with the dominant emission sectors in 2010 of transportation, industry, and residential, respectively. For both years, the emissions over the MICS-Asia regions contribute to over 40% of the global emissions. For these key O_3 precursors, the East Asian countries contribute to 45% (NMVOCs)-70% (NO_x) of the emissions in the MICS-Asia domain in both years, and the south Asian countries contribute to ~22% (NO_x)-34% (NMVOCs) of the MICS-Asia emissions. Non-anthropogenic emission inputs used in different models' simulations may differ. As this paper focuses on the impact of anthropogenic emissions, we do not introduce this information in detail.

2.2. Region definitions for the SR study and the model base and sensitivity simulations

2.2.1. Base and 20% emission perturbation simulations from global and regional models

Atmos. Chem. Phys. Discuss., doi:10.5194/acp-2016-958, 2016
Manuscript under review for journal Atmos. Chem. Phys.
Published: 28 November 2016

Atmospheric Chemistry and Physics Discussions

The HTAP2 simulations from eight global models, used in this study, are listed in Table 1a. Horizontal resolutions of these models range from finer than 1° to coarser than 2.5°, and overall these resolutions are higher than the HTAP1 participating models'. Relevant references for the RAQMS model and the SNU GEOS-Chem are Pierce et al. (2007, 2009) and Park et al. (2004) (with additional descriptions on its HTAP simulation configurations at: http://iek8wikis.iek.fz-juelich.de/HTAPWiki/WP2.3?action=AttachFile&do=view&target=_README_GEOS-Chem.pdf), respectively. The descriptions of the remaining models can be found in published HTAP2 works such as in Stjern et al. (2016). Figure 1 defines the source regions used in the HTAP2 SR relationship study and we will focus in this study on assessing the East Asia (EAS), S Asia (SAS), Europe (EUR), and non-NAM anthropogenic source (interchangeable in this paper with "(all) foreign") impacts on the NAM O_3 levels in 2010. Specifically, each model performed a base simulation and a number of sensitivity simulations in which the original HTAP2 anthropogenic emissions for all species and sectors in a defined source region were perturbed by a certain amount (referring to 20% as in most cases, unless specified differently) and these cases are defined in Table 1 as **source region**ALL (where "ALL" refers to "all species and sectors", consistent with HTAP1 and HTAP2's naming convention). The O_3 differences R(O_3, **source region**, **perturbation**) over the NAM were then calculated between each model's base and sensitivity simulations:

R(O_3, EAS, 20%) = BASE O_3-EASALL O_3 (1a)
R(O_3, SAS, 20%) = BASE O_3-SASALL O_3 (1b)
R(O_3, EUR, 20%) = BASE O_3-EURALL O_3 (1c)
R(O_3, non-NAM, 20%) = NAMALL O_3-GLOALL O_3 (1d)

The monthly-mean R(O_3, **source region**, 20%) values were averaged over the NAM region for the analysis and compared with the findings in the HTAP1 study (e.g., Fiore et al., 2009). It is worth mentioning that the rectangular source regions defined in HTAP1 were modified in HTAP2 to align with the geo-political borders. For EAS and SAS, the regions not overlapped by HTAP1 and HTAP2 are mostly in the less populated/polluted regions such as the northwestern China, according to the HTAP2 emission maps (http://edgar.jrc.ec.europa.eu/htap_v2/index.php). HTAP2's EUR domain excludes certain regions in Russia/Belarussia/Ukraine, Middle East and North Africa that are included in HTAP1's EUR domain. The impact of emissions over these regions on comparing the NAM R(O_3, EUR, 20%) values in HTAP1 and HTAP2 will be discussed in Section 3.2.1.

A unitless "Response to Extra-Regional Emission Reductions (RERER)" metric (Galmarini et al., 2016), as defined in eq. (2), was also calculated to measure the importance of local versus non-local sources to NAM's O_3 levels:

$$\text{RERER } (O_3, \text{NAM}) = \frac{R_{O3,non-NAM,20\%}}{R_{O3,global,20\%}} = \frac{(\text{NAMALL O3} - \text{GLOALL O3})}{(\text{BASE O3} - \text{GLOALL O3})} \quad (2)$$

The denominator and numerator terms of RERER represent the impacts of global and non-NAM anthropogenic emissions on NAM O_3, respectively. The higher the NAM RERER value is, the stronger impact from non-local sources on NAM is indicated. The RERER value can exceed 1, when emission reductions led to increasing concentrations (e.g. O_3 titration by nitrogen monoxide (NO)).

Atmos. Chem. Phys. Discuss., doi:10.5194/acp-2016-958, 2016
Manuscript under review for journal Atmos. Chem. Phys.
Published: 28 November 2016

Atmospheric Chemistry and Physics Discussions

The STEM (version 2K3) regional simulations were then performed on a 60 km×60 km horizontal resolution (a typical coarse regional model resolution) grid over NAM within the domain defined in Figure 2b during May-June 2010. The meteorological conditions in Spring 2010 were compared with the climatology from the NCEP/NCAR reanalysis data for the 1981-2010 period (Kalnay et al., 1996) in Huang et al. (2013b), concluding that this spring represents a period of stronger-than-climatological average spring trans-Pacific transport (based on a stronger meridional gradient in the North Pacific and higher Pacific/North American (PNA) indexes) and stratospheric intrusion conditions (based on the tropopause pressure and the UTLS relative humidity). The mean near-surface air temperatures in the western US in this spring were lower than the climatology, with larger anomalies in the mountain states, which may have led to weaker local O_3 production and decomposition of the transported peroxyacyl nitrates (PAN). In contrast, higher-than-normal temperatures were found in the eastern US that favored anomalously strong local O_3 production.

STEM has been used to interpret the observations collected by satellites and during aircraft campaigns in the past decade (e.g., Carmichael et al., 2003a, b; Huang et al., 2010, 2013a, b, 2014, 2015). STEM calculates gas-phase chemistry reactions based on the SAPRC 99 gaseous chemical mechanism (Carter, 2000) with thirty photolysis rates calculated online by the Tropospheric Ultraviolet-Visible radiation model (Madronich et al., 2002). Most of the key configurations of the 60 km base simulations are the same as those described in Lapina et al. (2014), i.e., meteorological fields were pre-calculated by the Advanced Research Weather Research and Forecasting Model (WRF-ARW, Skamarock et al., 2008) version 3.3.1 forced by the North American Regional Reanalysis data (Mesinger et al., 2006), using a similar set of the physics configuration to those in Huang et al. (2013a). Biomass burning emissions are from the Fire INventory from NCAR (FINN) inventory version 1.0 (Wiedinmyer et al., 2011). Biogenic emissions were calculated by the Model of Emissions of Gases and Aerosols from Nature (MEGAN) version 2.1 (Guenther et al., 2012), driven by the WRF meteorology. Lightning NO_x emissions are generated following the method in Allen et al. (2012), with the flash rates determined by the WRF convective precipitation and scaled to the National Lightning Detection Network flash rates. A major difference of the STEM simulations in this study from the Lapina (2014) study is that the anthropogenic emissions were replaced with the monthly-mean HTAP2 inventory with no weekday-weekend variability applied, rather than the earlier National Emission Inventory (NEI) 2005 in which the weekday-weekend variability exists. This change can introduce uncertainty, but was done to ensure consistency with the HTAP2 global model simulations, that also didn't use daily variable emissions for any regions. The VOC speciation for the SPRAC 99 chemical mechanism in the NEI 2005 (ftp://aftp.fsl.noaa.gov/divisions/taq/emissions_data_2005) were applied to break down the total NMVOC emissions provided in the HTAP2 inventory. The VOC speciation based on the year of 2005 can be unrealistic for 2005 as well as 2010 as studies have reported variable temporal changes of different VOC species in some US cities (e.g., Warneke et al., 2012). The time-varying lateral and top boundary conditions in the STEM base simulations were downscaled from three global models (i.e., 3 hourly SNU GEOS-Chem, 3 hourly ECMWF C-IFS, and 6 hourly RAQMS) base simulations. In support of the SR relationship study to quantify the East Asia anthropogenic impacts on the NAM, three STEM sensitivity simulations were also conducted in which the STEM boundary conditions were downscaled from the EASALL sensitivity simulations by these three global models (Table 1b). All STEM simulated 3D chemical fields were saved hourly for the convenience of calculating the US primary O_3 standard metric MDA8 as well as the quantitative

Atmos. Chem. Phys. Discuss., doi:10.5194/acp-2016-958, 2016
Manuscript under review for journal Atmos. Chem. Phys.
Published: 28 November 2016

Atmospheric Chemistry and Physics Discussions

comparisons against the satellite Level 2 (L2) O_3 products. The STEM base case surface O_3 performance and its O_3 sensitivities were also compared with those of its boundary condition models as well as the multi- global model means. The latitude/longitude ranges (20-50°N/130-65°W) of NAM for the global and regional model based sensitivity calculations were selected to mainly account for the coverage of the STEM domain, which are slightly different from the definition of North America in HTAP1.

2.2.2. Additional base and sensitivity simulations from selected models

In addition to the base and 20% EAS all-category emission perturbation simulations, the global RAQMS model conducted a sensitivity simulation in which the East Asian anthropogenic emissions were zeroed out, which was also used as STEM's boundary conditions (Table 1b). We calculate the "S_{O3}" metric (eq. (3)) using the O_3 sensitivities in STEM and RAQMS at the receptor regions in response to both 20% and 100% of emission reductions, to explore the relationships between the O_3 sensitivity and the size of the emission perturbation. A closer-to-one "S_{O3}" value indicates higher scalability of the sensitivity based on the 20% emission perturbation method for obtaining the full "contribution" of the East Asian anthropogenic emissions on the NAM O_3.

$$S_{O3} = R(O_3, EAS, 100\%)/R(O_3, EAS, 20\%)/5 \quad (3)$$

The RAQMS model also provided a base simulation that assimilated satellite O_3 products from the Ozone Monitoring Instrument (OMI, Levelt et al., 2006) and Microwave Limb Sounder (MLS, Livesey et al., 2008) (Pierce et al., 2007), which was used to help better understand the regional model base run error sources, as well as for demonstrating the use of satellite observations to help improve the representation of the trans-boundary pollution.

We also used a number of sensitivity simulations produced by the GEOS-Chem adjoint model v35f in which the emissions from selected anthropogenic emission sectors (power&industry, transportation, residential) or individual O_3 precursor chemical species (NO_x, VOC, CO) over the East Asia were reduced by 20%. Additional simulations for the 2008-2009 periods by the SNU GEOS-Chem were also utilized to quantify the East Asia and non-NAM anthropogenic source impacts in comparison with the 2010 conditions that we mainly focus on in this study.

2.3. In-situ and satellite observations

2.3.1. In-situ observations

The hourly O_3 observations at the Clean Air Status and Trends Network (CASTNET, http://epa.gov/castnet/javaweb/index.html) sites were used to evaluate the global and regional models' base simulations in four subregions: western US (i.e., the EPA regions 8, 9, 10); southern US (i.e., the EPA regions 4 and 6), the Midwest (i.e., the EPA regions 5 and 7), and the northeast (i.e., the EPA regions 1-3). The numbers of sites used in global and regional models' evaluation in each US subregion are summarized in Tables 2-3. The locations of these sites and the subregions they belong to are indicated in Figure 2b, overlaid on a model-based terrain height map. A majority of the CASTNET sites in the western US are located at high elevation (>1 km) remote or rural regions, more susceptible to the trans-boundary pollution (e.g., Jaffe, 2011). Most of the sites in the other three subregions are located in low elevation regions, mainly affected by local and

Atmos. Chem. Phys. Discuss., doi:10.5194/acp-2016-958, 2016
Manuscript under review for journal Atmos. Chem. Phys.
Published: 28 November 2016

Atmospheric Chemistry and Physics Discussions

regional pollution. The model-based terrain heights fairly well represent the reality on subregional scale – the differences between the actual and model-based subregional mean terrain heights at the CASTNET sites are smaller than 0.1 km (Table 3).

During May-June 2010, intense ozonesonde measurements were made at multiple California locations (Cooper et al., 2011), in support of the NOAA "California Nexus (CalNex): Research at the Nexus of Air Quality and Climate Change" field experiment (Ryerson et al., 2013). They have been used to evaluate the simulated O_3 vertical profiles by the HTAP2 participating models. The detailed evaluation results have been shown by Cooper et al. (2016), and will be covered by subsequent publications.

2.3.2. Satellite products

In a case study L2 and L3 O_3 and CO retrievals from several satellite instruments were used to assess the impacts of trans-Pacific pollution transport and stratospheric O_3 intrusions on NAM O_3 levels in early May. These include: 1) the early afternoon O_3 and CO profiles version 5 from the Tropospheric Emission Spectrometer (TES) (Beer et al., 2001; Beer, 2006) on the Aura satellite; 2) the mid-morning O_3 profiles from the METOP-Infrared Atmospheric Sounding Interferometer (IASI), which were retrieved using the Jet Propulsion Laboratory (JPL) TES optimal estimation retrieval algorithm (Bowman et al., 2006) for selected areas including the western US (Oetjen et al., 2014, 2016); as well as 3) the early afternoon L3 O_3 and CO maps (version 6, 1°×1°) from the Aqua Atmospheric Infrared Sounder (AIRS) instrument. The TES tropospheric O_3 retrieval is often sensitive to the mid- to lower free troposphere, and O_3 at these altitudes in the Eastern Pacific is known to possibly impact the downwind US surface air quality at later times (Huang et al., 2010; Parrish et al., 2010). TES O_3 is generally positively biased by <15% relative to high accuracy/precision reference datasets (e.g., Verstraeten et al., 2013). Although IASI is in general less sensitive than TES due to its coarse spectral resolution, the 681–316 hPa partial column-averaged O_3 mixing ratios in the JPL product agree well with TES O_3 for the 2008–2011 period with a -3.9 ppbv offset (Oetjen et al., 2016). Note that IASI O_3 data are processed operationally in Europe using a different algorithm. For this work we used O_3 profiles from TES and IASI processed using a consistent algorithm at JPL, although the latter set of data represents only a small subset of the full set of the IASI radiance measurements. The IASI and TES L2 O_3 profiles (screened by the retrieval quality and the C-Curve flags) were used to evaluate the STEM O_3 vertical distributions in the different base simulations, and the satellite observation operators were applied in these comparisons. Taking TES as an example, its observation operator h_z for O_3 is written in (4):

$$h_z = z_c + \mathrm{A_{TES}}\ (\ln(F_{TES}(c)) - z_c) \quad (4)$$

where z_c is the natural log form of the TES constraint vector (a priori) in volume mixing ratio. A_{TES} is the averaging kernel matrix reflecting the sensitivity of retrieval to changes in the true state (Rodgers, 2000). F_{TES} projects the modeled O_3 concentration fields c to the TES grid using spatial and temporal interpolation. The exponential of h_z is then used to compute the mismatches between the model and TES O_3 retrievals as the model evaluation. A small mismatch between model with the satellite observation operators and the satellite retrievals may indicate either good model performance or may be the low sensitivity of the retrievals to the true O_3 profile. AIRS O_3 is sensitive to the altitudes near the tropopause, with positive biases over the ozonesondes in the upper troposphere (e.g., Bian et al., 2007); AIRS CO is most sensitive to 300–600 hPa (Warner et

Atmos. Chem. Phys. Discuss., doi:10.5194/acp-2016-958, 2016
Manuscript under review for journal Atmos. Chem. Phys.
Published: 28 November 2016

Atmospheric Chemistry and Physics Discussions

al., 2007) and is frequently used together with the AIRS O_3 to distinguish the stratospheric O_3 intrusions from long-range transported anthropogenic or biomass burning pollution. We use the L3 AIRS products in this study to get a broad overview of the areas that are strongly impacted by the stratospheric O_3 intrusions or/and LRT of pollution.

The bottom-up NO_x emissions from the HTAP2 inventory were assessed on a monthly base by comparing the GEOS-Chem NO_2 columns with the de-stripped KNMI (Royal Netherlands Meteorological Institute) OMI column NO_2 product version 2.0 (Boersma et al., 2011a, b). For this model evaluation against the OMI L2 products, the NO_2 fields calculated by the GEOS-Chem adjoint model were saved daily at 13:30 local solar time, roughly coinciding with the Aura and Aqua overpassing times. Other parameters used in the model column calculations came from the GEOS-5/GEOS-Chem monthly mean conditions. The OMI data that passed the tropospheric quality flag at 13-14 local time were selected based on the following screening criteria: surface albedo<0.3; cloud fraction<0.2; solar zenith angle <75°; and viewing zenith angle <45°. The averaging kernels (Eskes and Boersma, 2003) and Air Mass Factors (AMFs) in the KNMI product were used to calculate the modeled tropospheric NO_2 vertical columns comparable to the OMI's. Details of the method to compare the model-based NO_2 columns with the KNMI OMI's can be found in Huang et al. (2014).

3. Results and Discussions

3.1. Evaluation of model base simulations and the HTAP2 bottom-up NO_x emissions

3.1.1. Evaluation of the global model O_3 ensembles and the bottom-up NO_x emissions

The monthly-mean surface O_3 from multiple global models' free runs was evaluated with the CASTNET observations, at the stations with 95% of the hourly O_3 observation completeness for the 1 May-30 June 2010 period, and the mean biases and RMSEs for these two months were summarized in Table 2 by US subregions. The three boundary condition-model as well as the eight-model ensembles overall underpredicted O_3 in the western US (by ~3-6 ppbv), similar to the HTAP1 model performance over these regions for May-June 2001. This can be due to the underestimated trans-boundary pollution (as indicated by the evaluation of modeled O_3 profiles with ozonesondes and satellite O_3 products). In addition, the coarser model resolutions are less capable of resolving the local features that influence the pollutants' import processes, chemical transformation, as well as regional processes such as the cross-state pollution transport over complex terrains. The global RAQMS base simulation with satellite assimilation improved the free tropospheric O_3 structure as its comparisons with the ozonesondes shows, which also enhanced the simulated monthly-mean surface O_3 by up to over 10 ppbv in the western US and some coastal areas in the southeastern US (Figure S1, left).

The global models overall significantly overestimated O_3 in the other subregions (by 8-12 ppbv), close to HTAP1 model performance for May-June 2001 over the similar areas (Fiore et al., 2009) and in the Lapina et al. (2014) study for 2010, in large part due to the uncertainties in the bottom-up emissions which will be discussed further in the following paragraphs. Satellite assimilation led to 2-6 ppbv higher RAQMS surface O_3 in the central/southern/eastern US than in its free simulation, which are associated with higher positive biases. Except in the northeastern US, the eight-model ensembles show better agreement with the CASTNET O_3 observations than the three boundary condition-model ensemble, suggesting that using a larger number of models in the

Atmos. Chem. Phys. Discuss., doi:10.5194/acp-2016-958, 2016
Manuscript under review for journal Atmos. Chem. Phys.
Published: 28 November 2016

Atmospheric Chemistry and Physics Discussions

ensemble calculations in this case may result in better overall model performance. The representation of land use/land cover, boundary layer mixing and chemistry in certain global model (i.e., GEOS-Chem) can be sources of uncertainty as reported in the literature (e.g., Geddes et al., 2016; Travis et al., 2016), but how serious these issues were in the other models need to be investigated further. Future work should emphasize on evaluating and comparing the models on process level to better understand the multi-model results.

The comparison of the GEOS-Chem adjoint NO_2 columns with the OMI product was used to help assess the bottom-up HTAP2 NO_x emissions. Figure 3 shows that NO_2 columns from GEOS-Chem's base simulations over the US are overall overestimated, and larger disagreement was found over the central/eastern US during June 2010. While grid-scale differences in NO_2 columns may not be directly indicative of emissions biases (Qu et al., 2016), overall there does appear to be a positive bias in the bottom-up emissions, mainly from the anthropogenic sources, consistent with the findings of Anderson et al. (2014) and Travis et al. (2016). The NO_2 columns in the GEOS-Chem base simulation were overestimated in many northern China rural areas and underpredicted in a few urban areas in the East Asia as well as a broad area in the southwestern China. The mismatches between model and OMI NO_2 fell within the ranges of the comparison between the GOME2 NO_2 column product and six models' simulations over China in summer 2008 (Quennehen et al., 2016). It is likely that other O_3 precursors' co-emitted with NO_x from the same sources are estimated with similar levels of uncertainties. Also, the use of monthly-mean anthropogenic emissions as well as the overall rough treatment of emission height and temporal profiles can be sources of uncertainty. These global model evaluation results suggest that the EAS-NAM SR relationships analyzed using this inventory may overall overestimate the NAM local contribution and underestimate the EAS contribution—This statement would also rely on the quality of other O_3 precursors in the HTAP2 emission inventory, so careful assessment of other key O_3 precursors' emissions in the inventory is also needed. Note that this comparison does not account for the biases in the used OMI data, and would be further validated by using other OMI NO_2 products as well as the bias-corrected (if applicable) in-situ NO_2 measurements. We recommend more global models to save their calculations more frequently, at least near the satellite overpassing times, for a more comprehensive assessment of the emission inventory.

3.1.2. Evaluation of the STEM regional base simulations w/ three sets of boundary conditions

The three STEM base simulations using different boundary conditions were averaged and evaluated with the hourly O_3 observations at the CASTNET sites in the four US subregions. The evaluation included the 8 May-30 June 2010 period to exclude the results during the one-week spin-up period. The evaluation statistics is summarized in Table 3. The time series of observed and modeled O_3 at the western US CASTNET sites are shown in Figure 2a where the model overall simulated the surface O_3 fairly well, with a much smaller mean bias (~1.6 ppbv) than the global model ensembles. However, this good performance can be a net effect of incorrect partitioning between the trans-boundary and local source contributions, with the former being underestimated and offsetting the overestimation of the latter. Switching the STEM chemical boundary conditions to the assimilated RAQMS base simulation led to increases in the simulated surface O_3 concentrations by >9 ppbv in the western US (Figure S1, right), associated with higher positive biases (due to several factors discussed in the next paragraph). Regional-scale assimilation could further reduce uncertainties introduced from regional meteorological and emission inputs to obtain

Atmos. Chem. Phys. Discuss., doi:10.5194/acp-2016-958, 2016
Manuscript under review for journal Atmos. Chem. Phys.
Published: 28 November 2016

Atmospheric Chemistry and Physics Discussions

better modeled total O_3 and the partitioning of trans-boundary versus US contributions (e.g., Huang et al., 2015).

The model significantly overpredicted O_3 over the rest of the US mainly due to the overall overestimated NO_x emissions. These positive biases are higher than the global model ensembles', which can partially result from the possible unrealistic VOC speciation of the emission inventory and the SAPRC 99 chemical mechanism: Although SAPRC mechanisms have been used in air quality modeling for regulatory applications in some US states such as California, they usually produced higher O_3 than other mechanisms such as the CB05 over the US, and the comparisons between SAPRC 99 and SAPRC 2007 are still in progress (e.g., Luecken et al., 2008; Zhang et al., 2012; Cai et al., 2011). It is important to timely update the chemical mechanisms in the chemistry models, and we also suggest to timely upgrade the VOC speciation in the bottom-up emission inventories in the US to benefit the air quality modeling. Additionally, the uncertainty from non-anthropogenic emissions, such as the biogenic VOC emissions from WRF/MEGAN which is known to often have positive biases, can be another cause: As Hogrefe et al. (2011) presented, the MEGAN emissions resulted in a higher O_3 response to hypothetical anthropogenic NO_x emission reductions compared with another set of biogenic emission input. Some factors that caused the overpredicted MEGAN emissions, such as positively-biased temperature in WRF, can also be important sources of uncertainty in the STEM modeled O_3. We anticipate that the results from the Air Quality Model Evaluation International Initiative (AQMEII) experiment (e.g., Schere et al., 2012; Solazzo et al., 2012; Galmarini et al., 2015, 2016), which involves other regional model simulations over the US with the similar set of boundary conditions but different chemical mechanisms and non-anthropogenic emission inputs, can help better understand the causes of errors in the simulated total O_3.

3.2. The NAM surface O_3 sensitivity to extra-regional anthropogenic pollutants

3.2.1. Global model ensembles

The impact of all foreign (i.e. non-NAM) anthropogenic sources on NAM surface O_3 was first explored, including the spatial distributions of the RERER metric (eq. (2)) based on various global models' simulations (Figure 4), and the domain wide mean sensitivities R (O_3, non-NAM, 20%) (eq. (1d)) (Figure 5). Across the NAM, the strongest impacts were found in spring time (March-April-May, larger than 1.5 ppbv in average over the domain) and the weakest impacts are shown during the summertime (June-July-August, 1.0-1.3 ppbv), consistent with the existing knowledge on the seasonal variability of the non-local pollution impacts on NAM for other years (e.g., Fiore et al., 2009; Reidmiller et al., 2009; Brown-Steiner and Hess, 2011). All global models indicate strong non-NAM anthropogenic source impacts on the western US mainly due to the impact of its high elevation, and also near the US-Mexico border areas, especially southern Texas, due to their vicinity to the Mexican emission sources. Over the western states, stronger non-local impacts were reflected from the results based on higher-resolution global models (e.g., the >0.6 RERER values from the half degree EMEP model, corresponding to its higher R(O_3, non-NAM, 20%) values than the other models'), similar to the findings in previous modeling studies (Lin et al., 2010, 2012a). Larger-than-1 RERER values are often seen near the urban areas and large point sources due to the titration, especially evident from the higher resolution model results. The R(O_3, EAS, 20%) values are larger than 1/3 of the R(O_3, non-NAM, 20%) (0.2-0.5 ppbv from April to June), more than 3-4 times higher than R(O_3, EUR, 20%) and R(O_3, SAS, 20%). Note that all eight

Atmos. Chem. Phys. Discuss., doi:10.5194/acp-2016-958, 2016
Manuscript under review for journal Atmos. Chem. Phys.
Published: 28 November 2016

Atmospheric Chemistry and Physics Discussions

552 models contributed to the R(O_3, EAS, 20%) calculations, but one or two models did not provide
553 all necessary sensitivity runs to compute the RERER, R(O_3, non-NAM, 20%), R(O_3, EUR, 20%),
554 or R(O_3, SAS, 20%).
555
556 Comparing to the HTAP1 modeling results, the magnitudes of R(O_3, EUR, 20%) are
557 smaller by a factor of 2-3, as a result of the substantial improvement in the European air quality
558 over the past decades (Crippa et al., 2016; Pouliot et al., 2015), and also possibly due to the changes
559 in the HTAP2 experiment setup from HTAP1 (e.g., EUR by HTAP1's definition includes regions
560 in Russia/Belarussia/Ukraine, Middle East and North Africa that are excluded from the HTAP2's
561 EUR domain). In contrast, the R(O_3, non-NAM, 20%) and R(O_3, EAS, 20%) values are >50%
562 higher than the HTAP1 modeling results. The R(O_3, EAS, 20%) based on the emission perturbation
563 approach are also larger than 1/5 of the original estimates (i.e., 1.94 ppbv and 0.79 ppbv for March-
564 April-May and June-July-August, respectively) for 2001-2005 using the tagged tracers (Brown-
565 Steiner and Hess, 2011) a method that produces a higher "contribution" than the emission
566 perturbation approach (e.g., Grewe et al., 2012; Emmons et al., 2012; Brown-Steiner and Hess,
567 2011). These results reflect the impact of the growing anthropogenic emissions from the East Asia
568 and other developing countries during 2001-2010. The SNU GEOS-Chem-based R(O_3, EAS, 20%)
569 and R(O_3, non-NAM, 20%) in Figure S2 both show that the NAM was a little more strongly
570 affected by foreign anthropogenic pollution in 2010 than in 2008-2009, especially in April-May.
571 This can be in part due to the higher O_3 precursors' emissions in 2010 from extra-regions including
572 the East Asia (Table S1). Such interannual variability can also be due to the Spring 2010
573 meteorological conditions that favored the trans-Pacific pollution transport, as introduced in
574 Section 2.2.1.
575
576 Similar to the findings from the HTAP1 studies, the large intermodel variability (as
577 indicated in Table 4) in the estimates of intercontinental SR relationships indicates the
578 uncertainties of these models in representing the key atmospheric processes which needs more
579 investigations in the future. Figure 5b compares the R (O_3, EAS, 20%) estimated by individual
580 boundary condition models, their ensemble mean sensitivities, and the eight-global model mean.
581 The averaged R(O_3, EAS, 20%) from the boundary condition model results are smaller than the
582 eight-global model mean, and GEOS-Chem gives higher R (O_3, EAS, 20%) than RAQMS and C-
583 IFS except for July-October 2010. The R (O_3, EAS, 20%) and the intermodel differences are
584 overall much smaller than the modeled total O_3 (<<5%) and their biases in NAM, as the impact of
585 the EAS anthropogenic sources has been diluted following transport over the great distances. Other
586 factors contribute more significantly to the biases in the modeled total O_3, such as the stratospheric
587 O_3 intrusions and the local O_3 formation, and controlling the local and regional emissions would
588 still be more effective for complying with the tighter air quality standard.
589
590 The O_3 sensitivities in response to the perturbations of individual species or sector
591 emissions in East Asia, estimated by the GEOS-Chem adjoint model, were also analyzed (Figure
592 S2). The EAS anthropogenic NO_x emissions more strongly impacted the NAM surface O_3 than the
593 other major O_3 precursors, similar to the findings in Fiore et al. (2009) and Reidmiller et al. (2009)
594 using the perturbation approach, as well as the conclusions in Lapina et al. (2014) based on the
595 adjoint sensitivity analyses. Emissions from the power&industrial sectors are higher in East Asia
596 than the other sectors (Table S1), resulting in its stronger influences on the NAM surface O_3. As
597 the observed NO_2 columns started to drop since 2010 due to the effective denitration devices

Atmos. Chem. Phys. Discuss., doi:10.5194/acp-2016-958, 2016
Manuscript under review for journal Atmos. Chem. Phys.
Published: 28 November 2016

Atmospheric Chemistry and Physics Discussions

implemented at the Chinese power and industrial plants (e.g., Liu et al., 2016), depending on the changes in the VOC emissions, it is anticipated to see different R (O_3, EAS, 20%) values for the years after 2010. Therefore, continued studies to assess the East Asian anthropogenic pollution impacts on NAM during more recent years is needed. As emissions from various source sectors can differ by their emitted altitudes and temporal (from diurnal to seasonal) profiles. Efforts should also be placed to have the models timely update the heights and temporal profiles of the emissions from those various sectors.

3.2.2. Regional model sensitivities and their connections with the boundary condition models'

The monthly-mean STEM surface R(O_3, EAS, 20%) sensitivities based on different boundary condition models were inter-compared, and also compared with the R(O_3, EAS, 20%) estimated by their boundary condition models as well as the global model ensemble mean (Figure 6). For both May and June 2010, the domain-wide mean R(O_3, EAS, 20%) values from STEM/RAQMS were higher than the estimates from RAQMS; the STEM/GEOS-Chem R(O_3, EAS, 20%) values are lower than those of GEOS-Chem, and the STEM/CIFS R(O_3, EAS, 20%) is higher than C-IFS's in June but slightly lower in May. These differences are overall smaller than the inter-global model differences, and can be due to various factors including the uncertainties in boundary condition chemical species mapping, and the different meteorological/terrain fields/chemistry in the global and regional models. The STEM R(O_3, EAS, 20%) ensemble mean values, however, are less than 0.02 ppbv different from its boundary condition model's ensemble mean for both months. The STEM R(O_3, EAS, 20%) ensemble mean value in June is also close to the eight-global model ensemble mean, but is ~0.05 ppbv lower than the eight-model mean in May. Choosing other/more global model outputs as STEM's boundary conditions may lead to different STEM ensemble mean R(O_3, EAS, 20%) estimates. We also found that the period mean R(O_3, EAS, 20%) of ~0.2 ppbv sampled only at the CASTNET sites (Table 3) are smaller than those averaged in all model grids. This indicates that currently the sparsely distributed surface network (especially over the western US that is more strongly affected by the extra-regional sources than the other US regions) may miss many LRT episodes that impact the NAM. The planned geostationary satellites with ~2-5 km footprint sizes and hourly sampling frequency (Hilsenrath and Chance, 2013) will help better capture the LRT episodes in these regions.

The spatial patterns of the monthly-mean STEM surface R(O_3, EAS, 20%) sensitivities based on the three boundary condition models are notably different, but overall resemble what's estimated by the corresponding boundary condition model, and the STEM sensitivities show more local details in certain high elevation regions in the US west (Figure 7 shows the June 2010 conditions as an example). These different sensitivities were investigated further, by examining the R(O_3, EAS, 20%) values near the source regions (i.e., East Asia) as well as near the receptor regions (Figure 8). More East Asian anthropogenic O_3 seems to be transported at the upper troposphere in RAQMS than in the other two models. GEOS-Chem and RAQMS R(O_3, EAS, 20%) sensitivities are similar over the EAS as well as the 500-900 hPa near the receptor in the eastern Pacific (at ~135°W), the altitudes US surface O_3 are most strongly sensitive to during the summertime as concluded from previous studies (e.g., Huang et al., 2010, 2013a; Parrish et al., 2010). Despite the close NAM domain-wide mean values from the STEM/GEOS-Chem and STEM/RAQMS, the spatial patterns of R(O_3, EAS, 20%) over NAM differ in these two cases, with the latter case showing sharper gradients especially in the western US, partially due to the

Atmos. Chem. Phys. Discuss., doi:10.5194/acp-2016-958, 2016
Manuscript under review for journal Atmos. Chem. Phys.
Published: 28 November 2016

Atmospheric Chemistry and Physics Discussions

644 impact of its higher horizontal resolution. The R(O_3, EAS, 20%) values from STEM/CIFS are
645 lower than from the other two cases both near the sources and at (near) NAM. The STEM surface
646 (also near surface, not shown in figures) R(O_3, EAS, 20%) does not spatially correlate well with
647 the column R(O_3, EAS, 20%), the latter of which contributed more to the base case O_3 columns,
648 indicating that a good portion of the transported East Asian pollution did not descend to the lower
649 altitudes to impact the boundary layer/ground level air quality. An additional regional simulation
650 was performed in which the STEM boundary conditions were downscaled from a RAQMS
651 simulation without the East Asian anthropogenic emissions. The non-linear emission perturbation-
652 O_3 response relationships, as the larger-than-1 S_{o3} metric (eq. (3)) indicate, are seen across the
653 domain, for both the surface and column O_3 (Figure 7). Therefore, the full source contribution
654 obtained by linearly scaling the receptor regional mean O_3 sensitivity to the 20% reduction in the
655 source region emissions may be underestimated.
656
657 The temporal variability of the STEM R(O_3, EAS, 20%) ensemble sensitivities were also
658 studied. For most US subregions, 3-6 LRT episodes (defined as when the sensitivities are above
659 the period mean) were identified during May-June. Throughout this period, the hourly R(O_3, EAS,
660 20%) and the observed O_3 at the surface CASTNET sites are weakly correlated (Table 3), but they
661 display similar diurnal cycles (e.g., Figure 2a for the western US sites), possibly because the deeper
662 boundary layer depth during the daytime enhanced entrainment down-mixing of the extra-regional
663 pollutants to the surface. The identified diurnal variability of the R(O_3, EAS, 20%) can cause
664 differences in the calculated MDA8 and all-hour mean R(O_3, EAS, 20%) values. Figure S3 shows
665 that the mean R(MDA8, EAS, 20%) values, usually at daytimes, are higher than the all-hour
666 averaged R(O_3, EAS, 20%) in most STEM model grids during both months. Therefore, it is
667 important for more HTAP2 participating models to save their outputs hourly in order to
668 conveniently compute the policy-relevant metrics for the O_3 sensitivities. Also, the hourly
669 sampling frequency of the planned geostationary satellites is anticipated to be more helpful for
670 evaluating the impacts of the LRT episodes.
671
672 The STEM R(MDA8, EAS, 20%) for May-June 2010 in four US subregions were averaged
673 on all days and only on the days when the simulated total MDA8 O_3 is over 70 ppbv (Figure 9).
674 These sensitivities also show appreciable spatial variability: from 0.35-0.58 ppbv in the western
675 US (also with the largest standard deviations, not shown), which is slightly higher than the HTAP1
676 results reported by Reidmiller et al. (2009) for Spring 2001, to ~0.1-0.25 ppbv in the rest three
677 subregions, which is close to the Reidmiller et al. (2009) results. Qualitatively consistent with the
678 findings in Reidmiller et al. (2009), R(MDA8, EAS, 20%) is smaller during the high O_3 total days
679 in all subregions. Note that the STEM base simulations overall substantially overpredicted the total
680 O_3 in non-western US regions, so the R(MDA8, EAS, 20%) calculated during the days of O_3
681 exceedances can actually represent the sensitivities during the non-exceedances.
682
683 *3.3. Case study of the 9 May 2010 LRT event mixed with stratospheric O_3 intrusions*
684
685 Lin et al. (2012a, b) and Neuman et al. (2012) showed that the trans-Pacific pollution
686 transport intensely impacted the western US during 8-10 May, 2010, intermingled with a
687 stratospheric intrusion. This episode is indeed indicated by the O_3 and CO products from AIRS
688 and TES at ~500 hPa over the E Pacific (Figure 10), and the observed TES and IASI O_3 profiles
689 over the western US indicated elevated O_3 levels (>80 ppbv) at 700-900 hPa. Huang et al. (2013b)

Atmos. Chem. Phys. Discuss., doi:10.5194/acp-2016-958, 2016
Manuscript under review for journal Atmos. Chem. Phys.
Published: 28 November 2016

Atmospheric Chemistry and Physics Discussions

found that the meteorological conditions during this period (i.e., a strong jet at ~700 hPa with wind speed >20 m/s shifted southwesterly when passing the southern California and continued to travel towards the mountain states), along with the orographic lifting, efficiently exported the southern California anthropogenic pollution, which was chemically coupled with the extra-regional pollution and significantly enhanced the O_3 levels in the US intermountain west.

We selected this episode to compare the STEM surface total O_3 concentrations as well as the R(O_3, EAS, 20%) sensitivities based on the different HTAP2 boundary condition models. Figure 11 evaluates the simulated O_3 profiles in the western US from several STEM base simulations against the TES and IASI O_3 retrievals, and Figures 12a-d indicate the performance of the daily surface total MDA8 O_3 from these simulations. We found that the underestimated free tropospheric O_3 from the STEM simulations that used any single free-running chemical boundary conditions contributed to the underestimated STEM surface O_3 in the high elevation mountain states. The STEM base simulation using the RAQMS assimilated fields as the boundary conditions, agrees most with the observed O_3 at the CASTNET sites, as well as the TES and IASI O_3 profiles in the western states. Similar to the conclusions drawn in Huang et al. (2010, 2015) for summer 2008, we again demonstrated the robustness of satellite chemical data assimilation for improving the boundary condition models' O_3 performance. As the enhancement of O_3 due to the assimilation is much larger than the O_3 sensitivities to the EAS anthropogenic emissions, the assimilation mainly improved the contributions from other sources, such as the stratospheric O_3.

The quality of the model boundary conditions only indicates how well the total "transported background" component is represented, and can not be directly connected with the accuracy of the model estimated R(O_3, EAS, 20%) sensitivities, which also show notable intermodel differences: The estimated R(MDA8, EAS, 20%) in the different STEM cases range from <1.0 ppbv to ~1.3 ppbv, at least 40% higher than the May-June period mean in Figure 9. Strong nonlinear emission perturbation-O_3 response relationships are also shown during this period (Figure 12, lower). The R(MDA8, EAS, 100%) from the STEM/RAQMS case is as high as >7 ppbv over the high terrain regions. These are of smaller magnitudes than the estimates in Lin et al. (2012a), possibly due to the differences in the used models and the bottom-up emission inputs.

A stratospheric O_3 intrusion also affected the NE US on the same day, as revealed by the satellite free tropospheric O_3 and CO observations (Figure 10). This intrusion was mixed with LRT East Asian pollution (Figure 12 and Figure S4). However, this intrusion did not enhance the NE boundary layer/surface O_3 concentrations, which were actually anomalously low (MDA8<40 ppbv) as indicated by the model base simulations and the CASTNET observations (Figure 12a-d). Similar characteristics during summertime stratospheric O_3 intrusion events around this region have been discussed by Ott et al. (2016). The East Asian pollution less intensely (<50%) affected the surface O_3 levels in these regions than in the US west, due to the greater transport distances as well as the impact of the overall flat terrain in the US east.

4. Conclusions and suggestions on future directions

In support of the HTAP Phase 2 experiment that involved high-resolution global models and regional models' participation to advance the understanding of the pollutants' SR relationships in the Northern Hemisphere, we conducted a number of regional scale STEM base and forward

Atmos. Chem. Phys. Discuss., doi:10.5194/acp-2016-958, 2016
Manuscript under review for journal Atmos. Chem. Phys.
Published: 28 November 2016

Atmospheric Chemistry and Physics Discussions

sensitivity simulations over North America during May-June 2010. The STEM top and lateral chemical boundary conditions were downscaled from three global models' (i.e., GEOS-Chem, RAQMS, and ECMWF CIFS) base and sensitivity simulations (in which the East Asian anthropogenic emissions were reduced by 20%). The STEM surface O_3 sensitivities (including the 24h mean and the policy-relevant MDA8 metric averaged throughout the study period and during a selected transport event) over North America overall resembled those from the corresponding boundary condition model, but can be quantitatively different from the mean sensitivities estimated by all global model ensembles. Therefore, choosing other/more global model outputs as STEM's boundary conditions may lead to different STEM ensemble mean O_3 sensitivities. Overall, the monthly-based US O_3 sensitivities to the 20% reduction of the East Asian anthropogenic emissions contributed to <<5% of the total O_3 and are of smaller magnitudes than the biases in the modeled total O_3. Better quantifying the contributions from other factors, such as the stratospheric O_3 intrusion and the local O_3 formation, would still be the most effective way to help reduce the North American pollution levels and the model uncertainties. The US O_3 sensitivities to the East Asian anthropogenic emissions were episodically strong, contributing to the O_3 exceedances in some high terrain areas. Assessing the sources of intermodel differences are particularly important for better evaluating the East Asian pollution impacts during these episodes. The STEM O_3 sensitivities followed similar diurnal cycles as the total O_3, emphasizing the importance of saving model results hourly for continently calculate policy-relevant metrics, as well as the usefulness of hourly sampling frequency of the planned geostationary satellites for better evaluating the impacts of the LRT events.

The ensemble mean O_3 sensitivities in 2010 were higher than the HTAP1 reported 2001 conditions, as well as 1/5 of the original estimates for 2001-2005 using the tagged tracers. This indicates the increasing impacts of the East Asian anthropogenic pollution on North America. The GEOS-Chem O_3 sensitivities in 2010 were also higher than the 2008-2009 conditions due to the increasing Asian emissions and the Spring 2010 meteorological conditions that favored the trans-Pacific pollution transport. The GEOS-Chem sensitivity calculations indicate that the East Asian anthropogenic NO_x emissions mattered more than the other East Asian O_3 precursors to the North American O_3, qualitatively consistent with previous adjoint sensitivity calculations. Continued research is needed on temporal changes of emissions for different species and sectors in North America and foreign countries as well as their impacts on the SR relationships. As emissions from various source sectors can differ by emitted altitudes and temporal profiles. Efforts should also be placed to have the models timely update the height and temporal profiles of the emissions from various sectors.

An additional STEM simulation was performed in which the boundary conditions were downscaled from a RAQMS simulation without East Asian anthropogenic emissions (i.e., a 100% emission reduction), to assess the scalability of the mean O_3 sensitivities to the size of the emission perturbation. The scalability was found to be spatially varying, and the full source contribution obtained by linearly scaling the NAM regional mean O_3 sensitivity to the 20% reduction in the East Asian emissions may be underestimated. Motivated by Lapina et al. (2014), additional calculations will be conducted in future to explore the scalability of different O_3 metrics in these cases. For future source attribution analysis, in general it is recommended to directly choose the suitable size of the emission perturbation based on the specific questions to address, and to avoid linearly scaling O_3 sensitivities that are based on other amounts of the perturbations.

Atmos. Chem. Phys. Discuss., doi:10.5194/acp-2016-958, 2016
Manuscript under review for journal Atmos. Chem. Phys.
Published: 28 November 2016

Atmospheric Chemistry and Physics Discussions

Satellite NO_2 (KNMI OMI) and O_3 (TES, JPL-IASI, OMI, MLS, and AIRS) products helped detect pollution episodes, quantify or/and reduce the uncertainties in the bottom-up NO_x emissions and the model transported background O_3. Based on model calculations and satellite/surface observations on a selected day of 9 May 2010, we showed the different influences from stratospheric O_3 intrusions along with the transported East Asian pollution on O_3 in the western and the eastern US. Continued studies on exceptional events during other seasons are in progress. As chemical data assimilation techniques keep developing (Bocquet et al., 2015), several HTAP2 participating global models have already been able to assimilate single- or multi-constitute satellite atmospheric composition data (e.g., Miyazaki et al., 2012; Parrington et al., 2008, 2009; Huang et al., 2015; Inness et al., 2015; Flemming et al., 2016). Comparing the performance of the assimilated fields from different models, and making the global model assimilated chemical fields in the suitable format for being used as boundary conditions would be very beneficial for future regional modeling, as well as for better interpreting the pollutants' distributions especially during the exceptional events. Meanwhile, efforts should also be devoted to advancing and applying higher-resolution regional scale modeling and chemical data assimilation. Furthermore, although satellite observations have been applied for improving the estimated US background O_3 (e.g., Huang et al., 2015), using satellite (and/or other types of) observations to improve SR relationship studies also needs to be explored. Some of the possible methods include: 1) The combination of data assimilation and the tagging approach; 2) Introducing observation-constrained emission estimates in the emission perturbation analyses.

Acknowledgements

The global and regional modeling results used in this study have been submitted to the AeroCom database following the HTAP2 data submission guidelines (http://iek8wikis.iek.fz-juelich.de/HTAPWiki/HTAP-2-data-submission), or can be made available upon request. Technical support from Anna Carlin Benedictow, Brigitte Koffi, Jan Griesfeller, and Michael Schulz regarding formatting and submitting the data to the AeroCom is acknowledged. MH thanks the research resources at the University of Iowa and JPL/Caltech that supported this study, as well as the travel funding from the US EPA for attending the related HTAP2 workshops. DKH and YD recognize support from NASA AQAST. Part of this research was carried out at the Jet Propulsion Laboratory, California Institute of Technology, under contract to the National Aeronautics and Space Administration. Reference herein to any specific commercial product, process or service by trade name, trademark, manufacturer or otherwise does not constitute or imply its endorsement by the United States Government or the Jet Propulsion Laboratory, California Institute of Technology. The views, opinions, and findings contained in this report are those of the author(s) and should not be construed as an official National Oceanic and Atmospheric Administration or U.S. Government position, policy, or decision.

Atmos. Chem. Phys. Discuss., doi:10.5194/acp-2016-958, 2016
Manuscript under review for journal Atmos. Chem. Phys.
Published: 28 November 2016

Atmospheric Chemistry and Physics Discussions

References

Anderson, D. C., Loughner, C. P., Diskin, G., Weinheimer, A., Canty, T., P., Salawitch, R. J., Worden, H. M., Fried, A., 25 Mikoviny, T., Wisthaler, A., and Dickerson, R., R. (2014), Measured and modeled CO and NO_y in DISCOVER-AQ: An evaluation of emissions and chemistry over the eastern US, Atmos. Environ., 96, 78-87, doi: 10.1016/j.atmosenv.2014.07.004.

Allen, D. J., Pickering, K. E., Pinder, R. W., Henderson, B. H., Appel, K. W., and Prados, A. (2012), Impact of lightning-NO on eastern United States photochemistry during the summer of 2006 as determined using the CMAQ model, Atmos. Chem. Phys., 12, 1737-1758, doi: 10.5194/acp-12-1737-2012.

Ambrose, J.L., Reidmiller, D.R., and Jaffe, D.A. (2011), Causes of high O_3 in the lower free troposphere over the Pacific Northwest as observed at the Mt. Bachelor Observatory. Atmos. Environ., 45, 5302–5315, doi: 10.1016/j.atmosenv.2011.06.056.

Anenberg, S. C., L. W. Horowitz, D. Q. Tong, and J. J. West (2010), An estimate of the global burden of anthropogenic ozone and fine particulate matter on premature human mortality using atmospheric modeling, Environ. Health Perspect., 118(9), 1189–1195.

Avnery, S, D.L. Mauzerall, J. Liu, L.W. Horowitz (2011a), Global Crop Yield Reductions due to Surface Ozone Exposure: 1. Year 2000 Crop Production Losses and Economic Damage, Atmos. Environ., 45, 2284-2296.

Avnery, S, D.L. Mauzerall, J. Liu, L.W. Horowitz (2011b), Global Crop Yield Reductions due to Surface Ozone Exposure: 2. Year 2030 Potential Crop Production Losses and Economic Damage under Two Scenarios of O_3 Pollution, Atmos. Environ., 45, 2297-2309.

Beer, R., T. A. Glavich, and D. M. Rider (2001), Tropospheric emission spectrometer for the Earth Observing System's Aura satellite, Applied Optics, 40, 2356 – 2367.

Beer, R (2006), TES on the Aura Mission: Scientific Objectives, Measurements, and Analysis Overview, IEEE Transaction on Geoscience and Remote Sensing, 44, 1102-1105.

Bian, J., A. Gettelman, H. Chen, and L. L. Pan (2007), Validation of satellite ozone profile retrievals using Beijing ozonesonde data, J. Geophys. Res., 112, D06305, doi:10.1029/2006JD007502.

Bocquet, M., Elbern, H., Eskes, H., Hirtl, M., Žabkar, R., Carmichael, G. R., Flemming, J., Inness, A., Pagowski, M., Pérez Camaño, J. L., Saide, P. E., San Jose, R., Sofiev, M., Vira, J., Baklanov, A., Carnevale, C., Grell, G., and Seigneur, C. (2015), Data assimilation in atmospheric chemistry models: current status and future prospects for coupled chemistry meteorology models, Atmos. Chem. Phys., 15, 5325-5358, doi:10.5194/acp-15-5325-2015.

Boersma, K. F., Braak, R., van der A, R. J. (2011a), Dutch OMI NO_2 (DOMINO) data product v2.0 HE5 data file user manual. http://www.temis.nl/docs/OMI_NO2_HE5_2.0_2011.pdf.

Boersma, K. F., Eskes, H. J., Dirksen, R. J., van der A, R. J., Veefkind, J. P., Stammes, P., Huijnen, V., Kleipool, Q. L., Sneep, M., Claas, J., Leitão, J., Richter, A., Zhou, Y., Brunner, D. (2011b), An improved tropospheric NO_2 column retrieval algorithm for the Ozone Monitoring Instrument, Atmos. Meas. Tech., 4, 1905-1928.

Bowman, K. W., Rodgers, C. D., Kulawik, S. S., Worden, J., Sarkissian, E., Osterman, G., Steck, T., Lou, M., Eldering, A., Shephard, M., Worden, H., Lampel, M., Clough, S., Brown, P., Rinsland, C., Gunson, M., and Beer, R. (2006), Tropospheric Emission Spectrometer: Retrieval method and error analysis, IEEE Transaction on Geoscience and Remote Sensing, 44 (5), 1297–1307, doi: 10.1109/TGRS.2006.871234.

866 Bowman, K., and D. K. Henze (2012), Attribution of direct ozone radiative forcing to spatially
867 resolved emissions, Geophys. Res. Lett., 39, L22704, doi:10.1029/2012GL053274.
868 Brown-Steiner, B., and P. Hess (2011), Asian influence on surface ozone in the United States: A
869 comparison of chemistry, seasonality, and transport mechanisms, J. Geophys. Res., 116,
870 D17309, doi:10.1029/2011JD015846.
871 Cai, C., J. T. Kelly, J. C. Avise, A. P. Kaduwela, and W. R. Stockwell (2011), Photochemical
872 Modeling in California with Two Chemical Mechanisms: Model Intercomparison and
873 Response to Emission Reductions, J. Air & Waste Manage. Assoc., 61:5, 559-572, doi:
874 10.3155/1047-3289.61.5.559.
875 Carmichael, G.R., Tang, Y., Kurata, G., Uno, I., Streets, D.G., Thongboonchoo, N., Woo, J.H.,
876 Guttikunda, S., White, A., Wang, T., Blake, D.R., Atlas, E., Fried, A., Potter, B., Avery, M.A.,
877 Sachse, G.W., Sandholm, S.T., Kondo, Y., Talbot, R.W., Bandy, A., Thorton, D., and Clarke,
878 A.D. (2003a), Evaluating regional emission estimates using the TRACE-P observations, J.
879 Geophys. Res., 108 (D21), 8810, doi: 10.1029/2002JD003116.
880 Carmichael, G.R., Tang, Y., Kurata, G., Uno, I., Streets, D., Woo, J.H., Huang, H., Yienger, J.,
881 Lefer, B., Shetter, R., Blake, D., Atlas, E., Fried, A., Apel, E., Eisele, F., Cantrell, C., Avery,
882 M., Barrick, J., Sachse, G., Brune, W., Sandholm, S., Kondo, Y., Singh, H., Talbot, R., Bandy,
883 A., Thorton, D., Clarke, A., and Heikes, B. (2003b), Regional-scale chemical transport
884 modeling in support of the analysis of observations obtained during the TRACE-P experiment,
885 J. Geophys. Res., 108 (D21), 8823, doi: 10.1029/2002JD003117.
886 Carter, W. P. L. (2000), Documentation of the SAPRC-99 chemical mechanism for VOC
887 Reactivity Assessment, final report to California Air Resources Board, Contract No. 92-329
888 and 95-308.
889 Cooper, O. R., et al. (2010), Increasing springtime ozone mixing ratios in the free troposphere over
890 western North America, Nature, 463, doi: 10.1038/nature08708.
891 Cooper, O. R., Oltmans, S. J., Johnson, B. J., Brioude, J., Angevine, W., Trainer, M., Parrish, D.
892 D., Ryerson, T. R., Pollack, I., Cullis, P. D., Ives, M. A., Tarasick, D. W., Al-Saadi, J., and
893 Stajner, I. (2011), Measurement of western U.S. baseline ozone from the surface to the
894 tropopause and assessment of downwind impact regions, J. Geophys. Res., 116, D00V03, doi:
895 10.1029/2011JD016095.
896 Cooper, O., et al. (2016), Western NA Performance Evaluation for HTAP2, HTAP2 workshop,
897 Potsdam, Germany, 2016.
898 Crippa, M., Janssens-Maenhout, G., Dentener, F., Guizzardi, D., Sindelarova, K., Muntean, M.,
899 Van Dingenen, R., and Granier, C. (2016), Forty years of improvements in European air
900 quality: regional policy-industry interactions with global impacts, Atmos. Chem. Phys., 16,
901 3825-3841, doi:10.5194/acp-16-3825-2016.
902 Emmons, L. K., Hess, P. G., Lamarque, J.-F., and Pfister, G. G. (2012), Tagged ozone mechanism
903 for MOZART-4, CAM-chem and other chemical transport models, Geosci. Model Dev., 5,
904 1531-1542, doi:10.5194/gmd-5-1531-2012.
905 Eskes, H. J. and Boersma, K. F. (2003), Averaging kernels for DOAS total-column satellite
906 retrievals, Atmos. Chem. Phys., 3, 1285-1291.
907 Fiore, A. M., et al. (2009), Multimodel estimates of intercontinental source receptor relationships
908 for ozone pollution, J. Geophys. Res., 114, D04301, doi:10.1029/2008JD010816.

909 Fiore, A. M., J. T. Oberman, M. Y. Lin, L. Zhang, O. E. Clifton, D. J. Jacob, V. Naik, L. W.
910 Horowitz, J. P. Pinto, and G. P. Milly (2014), Estimating North American background ozone
911 in U.S. surface air with two independent global models: Variability, uncertainties, and
912 recommendations, Atmos. Environ., 96, 284–300, doi: 10.1016/j.atmosenv.2014.07.045.
913 Flemming, J., Benedetti, A., Inness, A., Engelen, R., Jones, L., Huijnen, V., Remy, S., Parrington,
914 M., Suttie, M., Bozzo, A., Peuch, V.-H., Akritidis, D., and Katragkou, E. (2016), The CAMS
915 interim Reanalysis of Carbon Monoxide, Ozone and Aerosol for 2003–2015, Atmos. Chem.
916 Phys. Discuss., doi:10.5194/acp-2016-666, in review.
917 Galmarini, S., C. Hogrefe, D. Brunner, P. Makar, A. Baklanov (2015), Preface to the AQMEII p2
918 Special issue, Atmos. Environ., 115, 340-344.
919 Galmarini, S., Koffi, B., Solazzo, E., Keating, T., Hogrefe, C., Schulz, M., Benedictow, A.,
920 Griesfeller, J. J., Janssens-Maenhout, G., Carmichael, G., Fu, J., and Dentener, F. (2016),
921 Technical note: Harmonization of the multi-scale multi-model activities HTAP, AQMEII and
922 MICS-Asia: simulations, emission inventories, boundary conditions and output formats,
923 Atmos. Chem. Phys. Discuss., doi:10.5194/acp-2016-828, in review.
924 Geddes, J. A., Heald, C. L., Silva, S. J., and Martin, R. V. (2016), Land cover change impacts on
925 atmospheric chemistry: simulating projected large-scale tree mortality in the United States,
926 Atmos. Chem. Phys., 16, 2323-2340, doi:10.5194/acp-16-2323-2016.
927 Gratz, L.E., Jaffe, D.A., and Hee, J.R. (2014), Causes of increasing ozone and decreasing carbon
928 monoxide in springtime at the Mt. Bachelor Observatory from 2004 to 2013, Atmos. Environ.,
929 109, 323–330, doi: 10.1016/j.atmosenv.2014.05.076.
930 Grewe, V., Dahlmann, K., Matthes, S., and Steinbrecht, W. (2012), Attributing ozone to NOx
931 emissions: Implications for climate mitigation measures, Atmos. Environ., 59, 102-107, doi:
932 10.1016/j.atmosenv.2012.05.002.
933 Guenther, A. B., X. Jiang, C. L. Heald, T. Sakulyanontvittaya, T. Duhl, L. K. Emmons, and X.
934 Wang (2012), The Model of Emissions of Gases and Aerosols from Nature version 2.1
935 (MEGAN2.1): an extended and updated framework for modeling biogenic emissions, Geosci.
936 Model Dev., 5 (6), 1471-1492.
937 Hilsenrath, E., and K. Chance (2013), NASA ups the TEMPO on monitoring air pollution, Earth
938 Obs., 25, 10–15.
939 Hogrefe, C., Isukapalli, S., Tang, X., Georgopoulos, P., He, S., Zalewsky, E., Hao, W., Ku, J.,
940 Key, T., and Sistla, G. (2011), Impact of biogenic emission uncertainties on the simulated
941 response of ozone and fine Particulate Matter to anthropogenic emission reductions, J. Air
942 Waste Manage., 61, 92–108.
943 Huang, M., Carmichael, G. R., Adhikary, B., Spak, S. N., Kulkarni, S., Cheng, Y. F., Wei, C.,
944 Tang, Y., Parrish, D. D., Oltmans, S. J., D'Allura, A., Kaduwela, A., Cai, C.,
945 Weinheimer, A. J., Wong, M., Pierce, R. B., Al-Saadi, J. A., Streets, D. G., and Zhang, Q.
946 (2010), Impacts of transported background ozone on California air quality during the
947 ARCTAS-CARB period – a multi-scale modeling study, Atmos. Chem. Phys., 10, 6947-6968,
948 doi: 10.5194/acp-10-6947-2010.
949 Huang, M., Carmichael, G. R., Chai, T., Pierce, R. B., Oltmans, S. J., Jaffe, D. A.,
950 Bowman, K. W., Kaduwela, A., Cai, C., Spak, S. N., Weinheimer, A. J., Huey, L. G., and
951 Diskin, G. S. (2013a), Impacts of transported background pollutants on summertime western
952 US air quality: model evaluation, sensitivity analysis and data assimilation, Atmos. Chem.
953 Phys., 13, 359-391, doi: 10.5194/acp-13-359-2013.

954 Huang, M., Bowman, K. W., Carmichael, G. R., Pierce, R. B., Worden, H. M., Luo, M., Cooper,
955 O. R., Pollack, I. B., Ryerson, T. B., Brown, S. S. (2013b), Impact of southern California
956 anthropogenic emissions on ozone pollution in the mountain states, J. Geophys. Res., 118,
957 12784-12803, doi: 10.1002/2013JD020205.
958 Huang, M., et al. (2014), Changes in nitrogen oxides emissions in California during 2005–2010
959 indicated from top-down and bottom-up emission estimates, J. Geophys. Res., 119, 12,928–
960 12,952, doi: 10.1002/2014JD022268, 2014.
961 Huang, M., et al. (2015), Improved Western US Background Ozone Estimates via Constraining
962 Nonlocal and Local Source Contributions using Aura TES and OMI Observations, J. Geophys.
963 Res., 120, 3572–3592, doi: 10.1002/2014JD022993.
964 Inness, A., Blechschmidt, A.-M., Bouarar, I., Chabrillat, S., Crepulja, M., Engelen, R. J., Eskes,
965 H., Flemming, J., Gaudel, A., Hendrick, F., Huijnen, V., Jones, L., Kapsomenakis, J.,
966 Katragkou, E., Keppens, A., Langerock, B., de Mazière, M., Melas, D., Parrington, M., Peuch,
967 V. H., Razinger, M., Richter, A., Schultz, M. G., Suttie, M., Thouret, V., Vrekoussis, M.,
968 Wagner, A., and Zerefos, C. (2015), Data assimilation of satellite-retrieved ozone, carbon
969 monoxide and nitrogen dioxide with ECMWF's Composition-IFS, Atmos. Chem. Phys., 15,
970 5275-5303, doi:10.5194/acp-15-5275-2015.
971 Jaffe, D.A. (2011), Relationship between surface and free tropospheric ozone in the Western U.S.,
972 Environ. Sci. Technol., 45, 432–438, doi: 10.1021/es1028102.
973 Janssens-Maenhout, G., Crippa, M., Guizzardi, D., Dentener, F., Muntean, M., Pouliot, G.,
974 Keating, T., Zhang, Q., Kurokawa, J., Wankmüller, R., Denier van der Gon, H., Kuenen, J. J.
975 P., Klimont, Z., Frost, G., Darras, S., Koffi, B., and Li, M. (2015), HTAP_v2.2: a mosaic of
976 regional and global emission grid maps for 2008 and 2010 to study hemispheric transport of
977 air pollution, Atmos. Chem. Phys., 15, 11411-11432, doi:10.5194/acp-15-11411-2015.
978 Jerret, M., R. T. Burnett, C. A. Popo, III, K. Ito, G. Thurston, D. Krewski, Y. Shi, E. Calle, and M.
979 Thun (2009), Long-Term Ozone Exposure and Mortality, the New England Journal of
980 Medicine, 360, 1085-1096, doi: 10.1056/NEJMoa0803894.
981 Kalnay, E., and Co-authors (1996), The NCEP/NCAR 40-Year Reanalysis Project, Bulletin of the
982 American Meteorological Society, 77, 437–471.
983 Koffi, B., F. Dentener, G. Janssens-Maenhout, D. Guizzardi, M. Crippa, T. Diehl, S. Galmarini,
984 and E. Solazzo (2016), Hemispheric Transport Air Pollution (HTAP): Specification of the
985 HTAP2 experiments – Ensuring harmonized modelling, EUR - Scientific and Technical
986 Research Reports, in preparation.
987 Langford, A. O., Brioude, J., Cooper, O.R., Senff, C.J., Alvarez II, R.J., Hardesty, R.M., Johnson,
988 B.J., and Oltmans, S.J. (2011), Stratospheric influence on surface ozone in the Los Angeles
989 area during late spring and early summer of 2010, J. Geophys. Res. Atmos., 117, D00V06, doi:
990 10.1029/2011JD016766.
991 Lapina, K., D. K. Henze, J. B. Milford, M. Huang, M. Lin, A. M. Fiore, G. Carmichael, G. G.
992 Pfister, and K. Bowman (2014), Assessment of source contributions to seasonal vegetative
993 exposure to ozone in the U.S., J. Geophys. Res. Atmos., 119, 324–340,
994 doi:10.1002/2013JD020905.
995 Levelt, P.F., E. Hilsenrath, G.W. Leppelmeier, G.H.J. van den Oord, P.K. Bhartia, J. Tamminen,
996 J.F. de Haan and J.P. Veefkind (2006), Science Objectives of the Ozone Monitoring Instrument,
997 IEEE Transaction on Geoscience and Remote Sensing, 44, 1199-1208.
998 Li, M., Zhang, Q., Kurokawa, J., Woo, J.-H., He, K. B., Lu, Z., Ohara, T., Song, Y., Streets, D. G.,
999 Carmichael, G. R., Cheng, Y. F., Hong, C. P., Huo, H., Jiang, X. J., Kang, S. C., Liu, F., Su,

1000 H., and Zheng, B. (2015), MIX: a mosaic Asian anthropogenic emission inventory for the
1001 MICS-Asia and the HTAP projects, Atmos. Chem. Phys. Discuss., 15, 34813-34869,
1002 doi:10.5194/acpd-15-34813-2015.
1003 Lin, M., Holloway, T., Carmichael, G. R., and Fiore, A. M. (2010), Quantifying pollution inflow
1004 and outflow over East Asia in spring with regional and global models, Atmos. Chem. Phys.,
1005 10, 4221-4239, doi:10.5194/acp-10-4221-2010.
1006 Lin, M., A. M. Fiore, L. W. Horowitz, O. R. Cooper, V. Naik, J. Holloway, B. J. Johnson, A.
1007 Middlebrook, S. J. Oltmans, I. B. Pollack, T. B. Ryerson, J. X. Warner, C. Wiedinmyer, J.
1008 Wilson, B. Wyman (2012a), Transport of Asian ozone pollution into surface air over the
1009 western United States in spring, J. Geophys. Res., 117, D00V07, doi: 10.1029/2011JD016961.
1010 Lin, M., A. Fiore, O. R. R. Cooper, L. W. Horowitz, A. O. O. Langford, H. Levy II, B. J. Johnson,
1011 V. Naik, S. J. Oltmans, and C. J. Senff (2012b), Springtime high surface ozone events over the
1012 western United States: Quantifying the role of stratospheric intrusions, J. Geophys. Res., 117,
1013 D00V22, doi: 10.1029/2012JD018151.
1014 Livesey, N.J., M.J. Filipiak, L. Froidevaux, W.G. Read, A. Lambert, M.L. Santee, J.H. Jiang, H.C.
1015 Pumphrey, J.W. Waters, R.E. Cofield, D.T. Cuddy, W.H. Daffer, B.J. Drouin, R.A. Fuller, R.F.
1016 Jarnot, Y.B. Jiang, B.W. Knosp, Q.B. Li, V.S. Perun, M.J. Schwartz, W.V. Snyder, P.C. Stek,
1017 R.P. Thurstans, P.A. Wagner, M. Avery, E.V. Browell, J-P. Cammas, L.E. Christensen, G.S.
1018 Diskin, R-S. Gao, H-J. Jost, M. Loewenstein, J.D. Lopez, P. Nedelec, G.B. Osterman, G.W.
1019 Sachse, and C.R. Webster (2008), Validation of Aura Microwave Limb Sounder O3 and CO
1020 observations in the upper troposphere and lower stratosphere, J. Geophys. Res. 113, D15S02,
1021 doi:10.1029/2007JD008805.
1022 Liu, F., Q. Zhang, R. J. van der A, B. Zheng, D. Tong, L. Yan, Y. Zheng, and K. He (2016), Recent
1023 reduction in NO_x emissions over China: Synthesis of satellite observations and emission
1024 inventories, Environ. Res. Lett., 11 (11), 114002, doi: 10.1088/1748-9326/11/11/114002.
1025 Luecken, D.J., S. Phillips, G. Sarwar, C. Jang, Effects of using the CB05 vs. SAPRC99 vs. CB4
1026 chemical mechanism on model predictions (2008), Ozone and gas-phase photochemical
1027 precursor concentrations, Atmos. Environ., 42 (23), 5805-5820, doi:
1028 10.1016/j.atmosenv.2007.08.056.
1029 Maas, R. and P. Grennfelt (eds) (2016), Towards Cleaner Air Scientific Assessment Report 2016.
1030 EMEP Steering Body and Working Group on Effects of the Convention on Long-Range
1031 Transboundary Air Pollution, Oslo,
1032 http://www.unece.org/fileadmin/DAM/env/lrtap/ExecutiveBody/35th_session/CLRTAP_Scie
1033 ntific_Assessment_Report_-_Final_20-5-2016.pdf.
1034 Madronich, S., Flocke, S., Zeng, J., Petropavlovskikh, I., and Lee-Taylor, J. (2002), The
1035 Tropospheric Ultra-violet Visible (TUV) model Manual,
1036 https://www2.acom.ucar.edu/modeling/tropospheric-ultraviolet-and-visible-tuv-radiation-
1037 model.
1038 Mauzerall, D. L. and Wang, X. (2001), Protecting Agricultural Crops from the Effects of
1039 Tropospheric Ozone Exposure: Reconciling Science and Standard Setting in the United States,
1040 Europe and Asia, Annual Review of Energy and the Environment, 26, 237-268.
1041 McDonald-Buller, E. C., et al. (2011), Establishing policy relevant background (PRB) ozone
1042 concentrations in the United States, Environ. Sci. Technol., 45, 9484–9497.

1043 Mesinger, F., DiMego, G., Kalnay, E., Mitchell, K., Shafran, P. C., Ebisuzaki, W., Jovic, D.,
1044 Woollen, J., Rogers, E., Berbery, E. H., Ek, M. B., Fan, Y., Grumbine, R., Higgins, W., Li, H.,
1045 Lin, Y., Manikin, G., Parrish, D. and Shi, W. (2006), North American Regional Reanalysis,
1046 Bulletin of the American Meteorological Society, 87(3), 343–360, doi: 10.1175/BAMS-87-3-
1047 343.
1048 Miyazaki, K., Eskes, H. J., Sudo, K., Takigawa, M., van Weele, M., Boersma, K. F. (2012),
1049 Simultaneous assimilation of satellite NO_2, O_3, CO, and HNO_3 data for the analysis of
1050 tropospheric chemical composition and emissions, Atmos. Chem. Phys., 12, 9545-9579.
1051 Monks, P. S., Archibald, A. T., Colette, A., Cooper, O., Coyle, M., Derwent, R., Fowler, D.,
1052 Granier, C., Law, K. S., Mills, G. E., Stevenson, D. S., Tarasova, O., Thouret, V., von
1053 Schneidemesser, E., Sommariva, R., Wild, O., and Williams, M. L. (2015), Tropospheric
1054 ozone and its precursors from the urban to the global scale from air quality to short-lived
1055 climate forcer, Atmos. Chem. Phys., 15, 8889-8973, doi:10.5194/acp-15-8889-2015.
1056 National Research Council (NRC) (2009), global sources of local pollution-An Assessment of
1057 Long-Range Transport of Key Air Pollutants to and from the United States, 35-66,
1058 http://books.nap.edu/openbook.php?record_id=12743&page=35.
1059 Neuman, J. A., et al. (2012), Observations of ozone transport from the free troposphere to the Los
1060 Angeles basin, J. Geophys. Res. Atmos., 117, D00V09, doi: 10.1029/2011JD016919.
1061 Oetjen, H., Payne, V. H., Kulawik, S. S., Eldering, A., Worden, J., Edwards, D. P., Francis, G. L.,
1062 Worden, H. M., Clerbaux, C., Hadji-Lazaro, J., and Hurtmans, D. (2014), Extending the
1063 satellite data record of tropospheric ozone profiles from Aura-TES to MetOp-IASI:
1064 characterisation of optimal estimation retrievals, Atmos. Meas. Tech., 7, 4223–4236,
1065 doi:10.5194/amt-7-4223- 2014.
1066 Oetjen, H., Payne, V. H., Neu, J. L., Kulawik, S. S., Edwards, D. P., Eldering, A., Worden, H. M.,
1067 and Worden, J. R. (2016), A joint data record of tropospheric ozone from Aura-TES and
1068 MetOp-IASI, Atmos. Chem. Phys., 16, 10229-10239, doi:10.5194/acp-16-10229-2016.
1069 Ott, L. E., B. N. Duncan, A. M. Thompson, G. Diskin, Z. Fasnacht, A. O. Langford, M. Lin, A. M.
1070 Molod, J. E. Nielsen, S. E. Pusede, et al. (2016), Frequency and impact of summertime
1071 stratospheric intrusions over Maryland during DISCOVER-AQ (2011): New evidence from
1072 NASA's GEOS-5 simulations, J. Geophys. Res. Atmos., 121, 3687–3706,
1073 doi:10.1002/2015JD024052.
1074 Park, R. J., D. J. Jacob, B. D. Field, R. M. Yantosca, and M. Chin (2004), Natural and
1075 transboundary pollution influences on sulfate-nitrate-ammonium aerosols in the United States:
1076 Implications for policy, J. Geophys. Res., 109, D15204, doi:10.1029/2003JD004473.
1077 Parrington, M., D. B. A. Jones, K. W. Bowman, L. W. Horowitz, A. M. Thompson, D. W. Tarasick,
1078 and J. C. Witte (2008), Estimating the summertime tropospheric ozone distribution over North
1079 America through assimilation of observations from the Tropospheric Emission Spectrometer,
1080 J. Geophys. Res., 113, D18307, doi:10.1029/2007JD009341.
1081 Parrington, M., D. B. A. Jones, K. W. Bowman, A. M. Thompson, D. W. Tarasick, J. Merrill, S.
1082 J. Oltmans, T. Leblanc, J. C. Witte, and D. B. Millet (2009), Impact of the assimilation of
1083 ozone from the Tropospheric Emission Spectrometer on surface ozone across North America,
1084 Geophys. Res. Lett., 36, L04802, doi:10.1029/2008GL036935.
1085 Parrish, D. D., D. B. Millet, and A. H. Goldstein (2009), Increasing ozone in marine boundary
1086 layer inflow at the west coasts of North America and Europe, Atmos. Chem. Phys., 9, 1303–
1087 1323, doi:10.5194/acp-9-1303-2009.

1088 Parrish, D. D., Aikin, K. C., Oltmans, S. J., Johnson, B. J., Ives, M., and Sweeny, C. (2010), Impact
1089 of transported background ozone inflow on summertime air quality in a California ozone
1090 exceedance area, Atmos. Chem. Phys., 10, 10093-10109, doi:10.5194/acp-10-10093-2010.
1091 Parrish, D. D., et al. (2012), Long-term changes in lower tropospheric baseline ozone
1092 concentrations at northern mid-latitudes, Atmos. Chem. Phys., 12, 11,485–11,504,
1093 doi:10.5194/acp-12-11485-2012.
1094 Pierce, R. B., et al. (2007), Chemical data assimilation estimates of continental U.S. ozone and
1095 nitrogen budgets during the Intercontinental Chemical Transport Experiment–North America,
1096 J. Geophys. Res., 112, D12S21, doi:10.1029/2006JD007722.
1097 Pierce, R. B., et al. (2009), Impacts of background ozone production on Houston and Dallas, Texas,
1098 air quality during the Second Texas Air Quality Study field mission, J. Geophys. Res., 114,
1099 D00F09, doi:10.1029/2008JD011337.
1100 Pouliot, G., H. A.C. Denier van der Gon, J. Kuenen, J. Zhang, M. D. Moran, P.A. Makar (2015),
1101 Analysis of the emission inventories and model-ready emission datasets of Europe and North
1102 America for phase 2 of the AQMEII project, Atmos. Environ., 115, 345-360.
1103 Qu, Z., D. K. Henze, S. L. Capps, Y. Wang, X. Xu, J. Wang (2016), Monthly top-down NO_x
1104 emissions for China (2005-2012): a hybrid inversion method and trend analysis, submitted.
1105 Quennehen, B., Raut, J.-C., Law, K. S., Daskalakis, N., Ancellet, G., Clerbaux, C., Kim, S.-W.,
1106 Lund, M. T., Myhre, G., Olivié, D. J. L., Safieddine, S., Skeie, R. B., Thomas, J. L., Tsyro, S.,
1107 Bazureau, A., Bellouin, N., Hu, M., Kanakidou, M., Klimont, Z., Kupiainen, K.,
1108 Myriokefalitakis, S., Quaas, J., Rumbold, S. T., Schulz, M., Cherian, R., Shimizu, A., Wang,
1109 J., Yoon, S.-C., and Zhu, T. (2016), Multi-model evaluation of short-lived pollutant
1110 distributions over east Asia during summer 2008, Atmos. Chem. Phys., 16, 10765-10792,
1111 doi:10.5194/acp-16-10765-2016.
1112 Reidmiller, D. R., Fiore, A. M., Jaffe, D. A., Bergmann, D., Cuvelier, C., Dentener, F. J., Duncan,
1113 B. N., Folberth, G., Gauss, M., Gong, S., Hess, P., Jonson, J. E., Keating, T., Lupu, A., Marmer,
1114 E., Park, R., Schultz, M. G., Shindell, D. T., Szopa, S., Vivanco, M. G., Wild, O., and Zuber,
1115 A. (2009), The influence of foreign vs. North American emissions on surface ozone in the US,
1116 Atmos. Chem. Phys., 9, 5027-5042, doi:10.5194/acp-9-5027-2009.
1117 Rodgers, C. D. (2000), Inverse Methods for Atmospheric Sounding: Theory and Practice, World
1118 Sci., Singapore.
1119 Ryerson, T. B., Andrews, A. E., Angevine, W. M., Bates, T. S., Brock, C. A., Cairns, B., Cohen,
1120 R. C., Cooper, O. R., de Gouw, J. A., Fehsenfeld, F. C., Ferrare, R. A., Fischer, M. L., Flagan,
1121 R. C., Goldstein, A. H., Hair, J. W., Hardesty, R. M., Hostetler, C. A., Jimenez, J. L., Langford,
1122 A. O., McCauley, E., McKeen, S. A., Molina, L. T., Nenes, A., Oltmans, S. J., Parrish, D. D.,
1123 Pederson, J. R., Pierce, R. B., Prather, K., Quinn, P. K., Seinfeld, J. H., Senff, C. J., Sorooshian,
1124 A., Stutz, J., Surratt, J. D., Trainer, M., Volkamer, R., Williams, E. J., Wofsy, S. C. (2013),
1125 The 2010 California Research at the Nexus of Air Quality and Climate Change (CalNex) field
1126 study, J. Geophys. Res., 118, 5830–5866.
1127 Schere, K. J. Flemming, R. Vautard, C. Chemel, A. Colette, C. Hogrefe, B. Bessagnet, F. Meleux,
1128 R. Mathur, S. Roselle, R.-M. Hu, R. S. Sokhi, S. T. Rao, S. Galmarini (2012), Trace gas/aerosol
1129 boundary concentrations and their impacts on continental-scale AQMEII modeling domains,
1130 Atmos. Environ., 53, 38-50, doi: 10.1016/j.atmosenv.2011.09.043.
1131 Shindell, D. T., G. Faluvegi, D. M. Koch, G. A. Schmidt, N. Unger, and S. E. Bauer (2009),
1132 Improved attribution of climate forcing to emissions, Science, 326, 716–718, doi:
1133 10.1126/science.1174760.

1134 Shindell, D. T., et al. (2013), Radiative forcing in the ACCMIP historical and future climate
1135 simulations, Atmos. Chem. Phys., 13, 2939–2974, doi:10.5194/acp-13-2939-2013.
1136 Skamarock, W. C., J. B. Klemp, J. Dudhia, D. Gill, D. M. Barker, W. Wang, and J. G. Powers
1137 (2008), A description of the Advanced Research WRF version 3 (Available at
1138 www.mmm.ucar.edu/wrf/users/docs/arwv3.pdf).
1139 Smith, K. R., Jerrett, M., and Anderson, H. R. et al. (2009), Public health benefits of strategies to
1140 reduce greenhouse-gas emissions: health implications of short-lived greenhouse pollutants,
1141 Lancet, doi: 10.1016/S0140-6736 (09) 61716-5.
1142 Solazzo, E. R. Bianconi, R. Vautard, K. W. Appel, M. D. Moran, C. Hogrefe, B. Bessagnet, J.
1143 Brandt, J. H. Christensen, C. Chemel, I. Coll, H. D. van der Gon, J. Ferreira, R. Forkel, X. V.
1144 Francis, G. Grell, P. Grossi, A. B. Hansen, A. Jeričević, L. Kraljević, A. I. Miranda, U.
1145 Nopmongcol, G. Pirovano, M. Prank, A. Riccio, K. N. Sartelet, M. Schaap, J. D. Silver, R. S.
1146 Sokhi, J. Vira, J. Werhahn, R. Wolke, G. Yarwood, J. Zhang, S.T. Rao, S. Galmarini (2012),
1147 Model evaluation and ensemble modelling of surface-level ozone in Europe and North
1148 America in the context of AQMEII, Atmos. Environ., 53, 60-74, , doi:
1149 10.1016/j.atmosenv.2012.01.003.
1150 Stevenson, D. S., et al. (2006), Multimodel ensemble simulations of present-day and near-future
1151 tropospheric ozone, J. Geophys. Res., 111, D08301, doi:10.1029/2005JD006338.
1152 Stevenson, D. S., et al. (2013), Tropospheric ozone changes, radiative forcing and attribution to
1153 emissions in the Atmospheric Chemistry and Climate Model Intercomparison Project
1154 (ACCMIP), Atmos. Chem. Phys., 13, 3063–3085, doi:10.5194/acp-13-3063-2013.
1155 Stjern, C. W., Samset, B. H., Myhre, G., Bian, H., Chin, M., Davila, Y., Dentener, F., Emmons,
1156 L., Flemming, J., Haslerud, A. S., Henze, D., Jonson, J. E., Kucsera, T., Lund, M. T., Schulz,
1157 M., Sudo, K., Takemura, T., and Tilmes, S. (2016), Atmos. Chem. Phys., 16, 13579-13599,
1158 doi:10.5194/acp-16-13579-2016.
1159 Susaya, J., Kim, K.-H., Shon, Z.-H., Brown R. J. (2013), Demonstration of long-term increases in
1160 tropospheric O_3 levels: Causes and potential impacts, Chemosphere, 92, 1520–1528.
1161 Task Force on Hemispheric Transport of Air Pollution (HTAP) (2010), 2010 Final Assessment
1162 report, Part A: Ozone and particulate matter,
1163 http://www.htap.org/activities/2010_Final_Report/HTAP%202010%20Part%20A%2011040
1164 7.pdf.
1165 Travis, K. R., Jacob, D. J., Fisher, J. A., Kim, P. S., Marais, E. A., Zhu, L., Yu, K., Miller, C. C.,
1166 Yantosca, R. M., Sulprizio, M. P., Thompson, A. M., Wennberg, P. O., Crounse, J. D., St.
1167 Clair, J. M., Cohen, R. C., Laugher, J. L., Dibb, J. E., Hall, S. R., Ullmann, K., Wolfe, G. M.,
1168 Pollack, I. B., Peischl, J., Neuman, J. A., and Zhou, X. (2016), Why do models overestimate
1169 surface ozone in the Southeast United States?, Atmos. Chem. Phys., 16, 13561-13577,
1170 doi:10.5194/acp-16-13561-2016.
1171 United Nations Environment Programme and World Meteorological Organization (2011),
1172 Integrated Assessment of Black Carbon and Tropospheric Ozone: Summary for Decision
1173 Makers, http://www.unep.org/dewa/Portals/67/pdf/Black_Carbon.pdf.
1174 US EPA (2016a), Implementation of the 2015 Primary Ozone NAAQS: Issues Associated with
1175 Background Ozone White Paper for Discussion,
1176 https://www.epa.gov/sites/production/files/2016-03/documents/whitepaper-bgo3-final.pdf.
1177 US EPA (2016b), High level summary of background ozone workshop,
1178 https://www.epa.gov/sites/production/files/2016-03/documents/bgo3-high-level-
1179 summary.pdf.

1180 Verstraeten, W. W., K. F. Boersma, J. Zörner, M. A. F. Allaart, K. W. Bowman, and J. R. Worden
1181 (2013), Validation of six years of TES tropospheric ozone retrievals with ozonesonde
1182 measurements: Implications for spatial patterns and temporal stability in the bias, Atmos. Meas.
1183 Tech., 6, 1413–1423.
1184 Verstraeten, W.W., J. L. Neu, J. E. Williams, K. W. Bowman, J. R. Worden, and K. F. Boersma
1185 (2015), Rapid increases in tropospheric ozone production and export from China, Nature
1186 Geoscience, 8, 690–695, doi:10.1038/ngeo2493.
1187 Wang, Y., Konopka, P., Liu, Y., Chen, H., Müller, R., Plöger, F., Riese, M., Cai, Z., and Lü, D.
1188 (2012), Tropospheric ozone trend over Beijing from 2002–2010: ozonesonde measurements
1189 and modeling analysis, Atmos. Chem. Phys., 12, 8389-8399, doi:10.5194/acp-12-8389-2012.
1190 Warneke, C., J. A. deGouw, J. S. Holloway, J. Peischl, T. B. Ryerson, E. Atlas, D. Blake, M.
1191 Trainer, and D. D. Parrish (2012), Multiyear trends in volatile organic compounds in Los
1192 Angeles, California: Five decades of decreasing emissions, J. Geophys. Res., 117, D00V17,
1193 doi:10.1029/2012JD017899.
1194 Warner, J. X., McCourt Comer, M., Barnet, C. D., McMillan, W. W., Wolf, W., Maddy, E., and
1195 Sachse, G. (2007), A comparison of satellite tropospheric carbon monoxide measurements
1196 from AIRS and MOPITT during INTEX-A, J. Geophys. Res., 112, D12S17,
1197 doi:10.1029/2006JD007925, 2007.
1198 Wiedinmyer, C., Akagi, S. K., Yokelson, R. J., Emmons, L. K., Al-Saadi, J. A., Orlando, J. J., and
1199 Soja, A. J. (2011), The Fire INventory from NCAR (FINN): a high resolution global model to
1200 estimate the emissions from open burning, Geosci. Model Dev., 4, 625-641, doi:10.5194/gmd-
1201 4-625-2011.
1202 Wigder, N.L., Jaffe, D.A., Herron-Thorpe, F.L., and Vaughan, J.K. (2013), Influence of daily
1203 variations in baseline ozone on urban air quality in the United States Pacific Northwest, J.
1204 Geophys. Res., 118, 3343–3354, doi: 10.1029/2012JD018738.
1205 Wild, O., Fiore, A. M., Shindell, D. T., Doherty, R. M., Collins, W. J., Dentener, F. J., Schultz, M.
1206 G., Gong, S., MacKenzie, I. A., Zeng, G., Hess, P., Duncan, B. N., Bergmann, D. J., Szopa,
1207 S., Jonson, J. E., Keating, T. J., and Zuber, A. (2012), Modelling future changes in surface
1208 ozone: a parameterized approach, Atmos. Chem. Phys., 12, 2037-2054, doi:10.5194/acp-12-
1209 2037-2012.
1210 Wu, S., B. N. Duncan, D. J. Jacob, A. M. Fiore, and O. Wild (2009), Chemical nonlinearities in
1211 relating intercontinental ozone pollution to anthropogenic emissions, Geophys. Res. Lett., 36,
1212 L05806, doi:10.1029/2008GL036607.
1213 Zhang, L., Jacob, D. J., Boersma, K. F., Jaffe, D. A., Olson, J. R., Bowman, K. W., Worden, J. R.,
1214 Thompson, A. M., Avery, M. A., Cohen, R. C., Dibb, J. E., Flock, F. M., Fuelberg, H. E.,
1215 Huey, L. G., McMillan, W. W., Singh, H. B., and Weinheimer, A. J. (2008), Transpacific
1216 transport of ozone pollution and the effect of recent Asian emission increases on air quality in
1217 North America: an integrated analysis using satellite, aircraft, ozonesonde, and surface
1218 observations, Atmos. Chem. Phys., 8, 6117-6136, doi:10.5194/acp-8-6117-2008.
1219 Zhang, L., Jacob, D. J., Kopacz, M., Henze, D. K., Singh, K., and Jaffe, D. A. (2009),
1220 Intercontinental source attribution of ozone pollution at western U.S. sites using an adjoint
1221 method, Geophys. Res. Lett., 36, L11810, doi: 10.1029/2009GL037950.
1222 Zhang, L., D. J. Jacob, N. V. Downey, D. A. Wood, D. Blewitt, C. C. Carouge, A. van Donkelaar,
1223 D. B. A. Jones, L. T. Murray, and Y. Wang (2011), Improved estimate of the policy-relevant
1224 background ozone in the United States using the GEOS-Chem global model with 1/2°×2/3°

1225 horizontal resolution over North America, Atmos. Environ., 45, 6769–6776, doi:
1226 10.1016/j.atmosenv.2011.07.054.
1227 Zhang, Q., Yuan, B., Shao, M., Wang, X., Lu, S., Lu, K., Wang, M., Chen, L., Chang, C.-C., and
1228 Liu, S. C. (2014), Variations of ground-level O_3 and its precursors in Beijing in summertime
1229 between 2005 and 2011, Atmos. Chem. Phys., 14, 6089-6101, doi:10.5194/acp-14-6089-2014.
1230 Zhang, Y., Y. Chen, G. Sarwar, and K. Schere (2012), Impact of gas-phase mechanisms on
1231 Weather Research Forecasting Model with Chemistry (WRF/Chem) predictions: Mechanism
1232 implementation and comparative evaluation, J. Geophys. Res., 117, D01301,
1233 doi:10.1029/2011JD015775.

Atmos. Chem. Phys. Discuss., doi:10.5194/acp-2016-958, 2016
Manuscript under review for journal Atmos. Chem. Phys.
Published: 28 November 2016

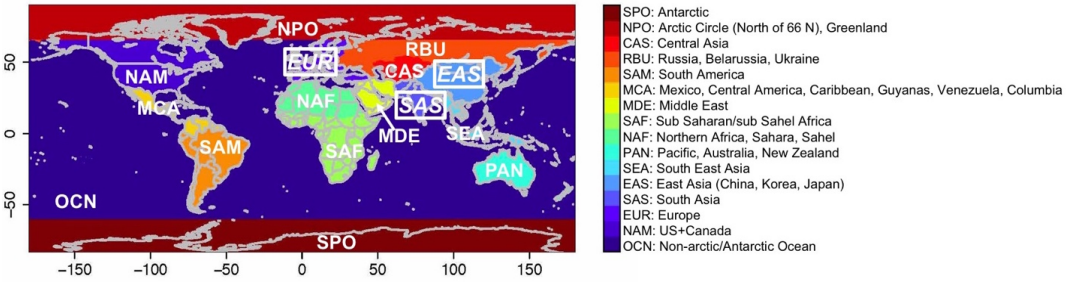

Figure 1. Definitions of the 16 source regions used in HTAP2 SR relationship study. The map is plotted based on data on a 0.1°×0.1° resolution grid. We focus in this study on the impact of anthropogenic pollution from selected non-North American source regions (i.e., EAS, SAS, and EUR), as highlighted in italic.

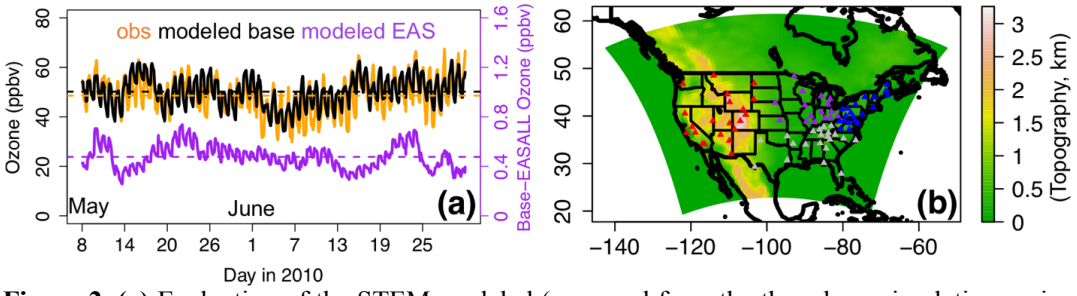

Figure 2. (a) Evaluation of the STEM modeled (averaged from the three base simulations using the GEOS-Chem, ECMWF C-IFS, and RAQMS base runs as the chemical boundary conditions) hourly O_3 at the western US (i.e., EPA regions 8, 9, and 10) CASTNET sites. Observations, modeled base O_3 and the modeled R(O_3, EAS, 20%) are in orange, black, and purple lines, respectively. The horizontal dashed lines indicate the period mean values. **(b)** The 60 km STEM NAM domain, colored by the model topography. The CASTNET sites used in the STEM base O_3 evaluation are marked as triangles in different colors that identify the subregions they belong to (red: western US; grey: southern US; purple: Midwest; blue: northeastern US).

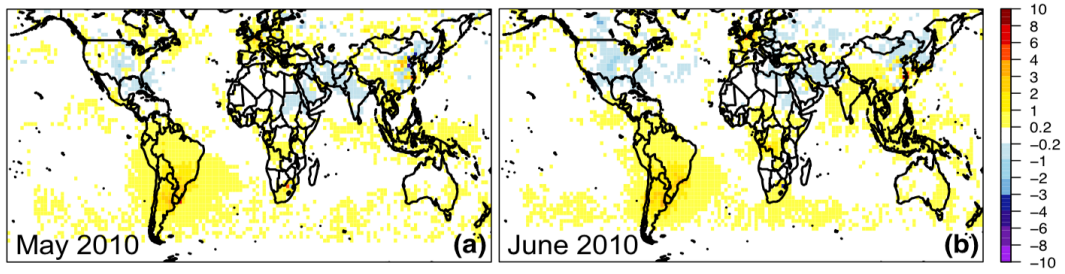

Figure 3. Evaluation of the GEOS-Chem adjoint base NO_2 product (recorded at near the satellite overpassing time) with the OMI NO_2 columns. The differences between OMI and GEOS-Chem (OMI-modeled) tropospheric NO_2 columns ($\times 10^{15}$ molec./cm^2) are shown for **(a)** May and **(b)** June 2010. Details of the comparison are included in Section 2.3.2.

Atmos. Chem. Phys. Discuss., doi:10.5194/acp-2016-958, 2016
Manuscript under review for journal Atmos. Chem. Phys.
Published: 28 November 2016

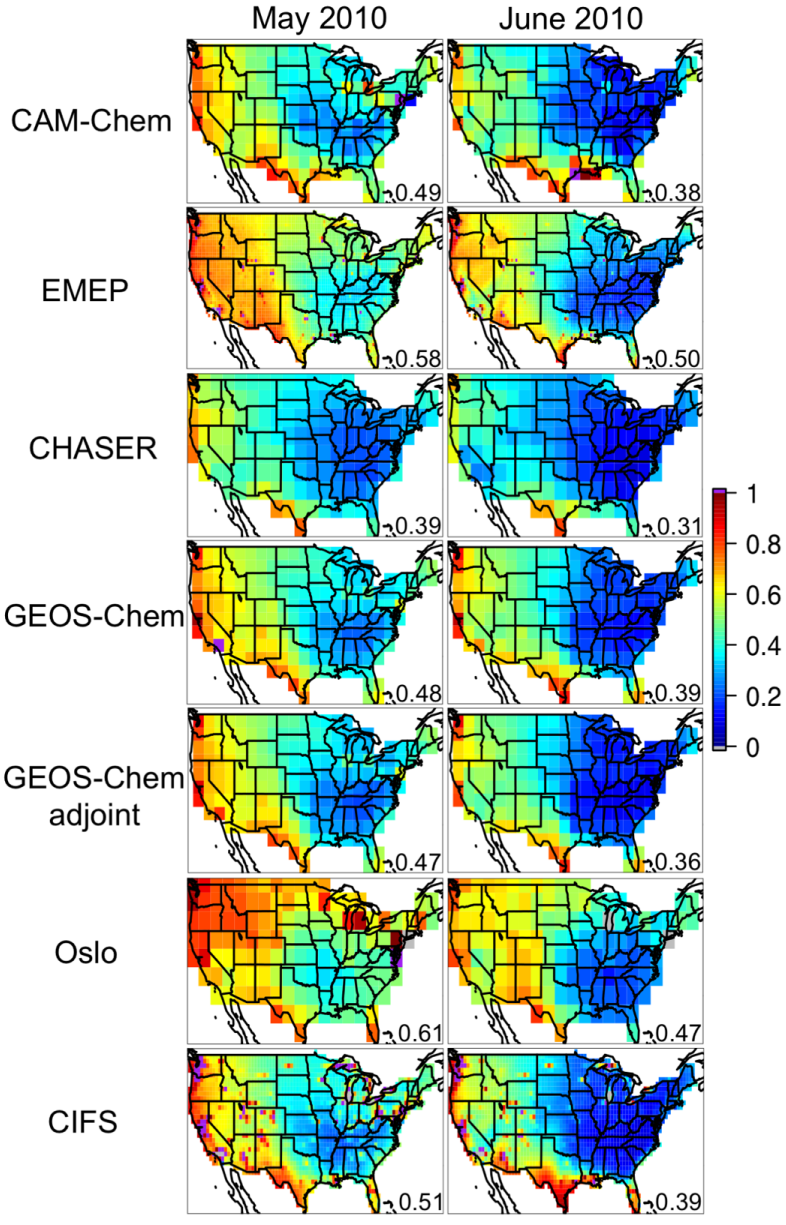

Figure 4. The RERER maps in May (left) and June (right) 2010 over the continental US, calculated based on the monthly mean O_3 from multiple global models' base and emission sensitivity simulations. The RERER metric (unitless) was defined in eq. (2) in the text. Values larger than 1 and smaller than 0 are shown in purple and grey, respectively. The US (including continental US as well as Hawaii which is not shown in the plots) mean values are indicated for each panel at the lower right corner. The 7-model mean RERER values for May and June 2010 are ~0.5 and ~0.4, respectively.

Atmos. Chem. Phys. Discuss., doi:10.5194/acp-2016-958, 2016
Manuscript under review for journal Atmos. Chem. Phys.
Published: 28 November 2016

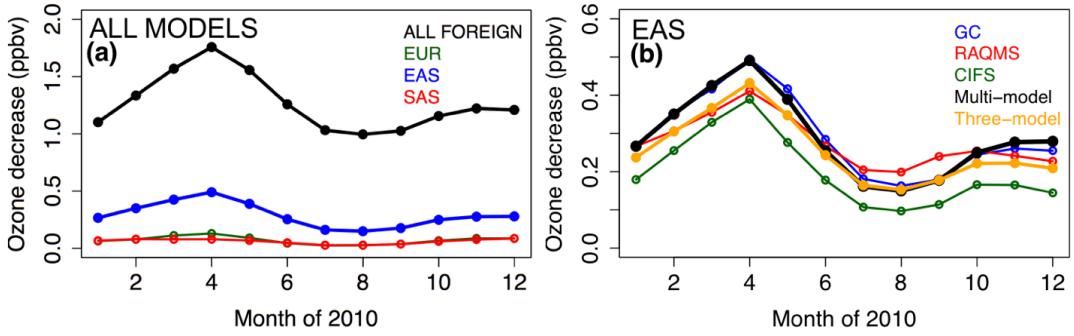

Figure 5. (a) North American (130-65°W; 20-50°N) mean O_3 sensitivity to 20% anthropogenic emission reductions in various non-North American regions, averaged from multiple (six-eight, see details in text) global models. **(b)** North American surface R(O_3, EAS, 20%) values, as estimated by single (the three STEM boundary condition models) or multi- global model means. The "Multi-model" and "Three-model" in the legend indicate the mean sensitivities of all eight global models and only of the three boundary condition models, respectively.

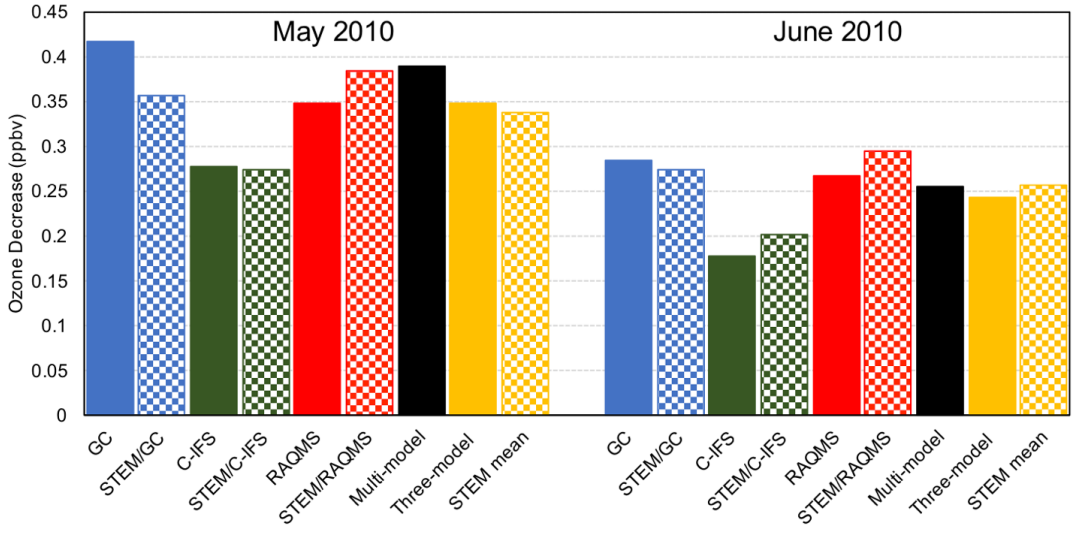

Figure 6. Monthly-mean North American (130-65°W; 20-50°N) surface R(O_3, EAS, 20%) values from multiple global and regional model simulations for May (left) and June (right) 2010. STEM model mean values were calculated from its hourly output from 8 May and on. The "Multi-model" and "Three-model" in the legend indicate the mean sensitivities of all eight global models and only of the three boundary condition models, respectively.

Atmos. Chem. Phys. Discuss., doi:10.5194/acp-2016-958, 2016
Manuscript under review for journal Atmos. Chem. Phys.
Published: 28 November 2016

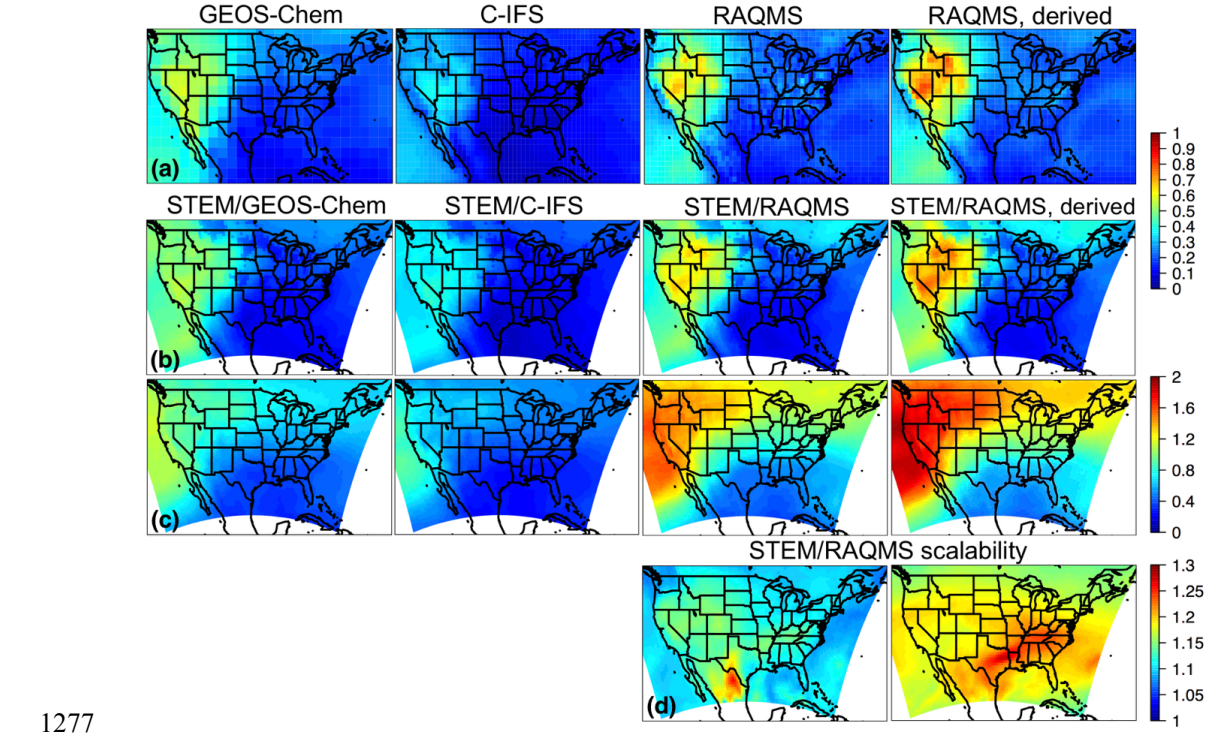

Figure 7. The monthly-mean R(O_3, EAS, 20%) in June 2010 for: **(a)** surface O_3 (ppbv) from the three boundary condition models, **(b)** STEM surface O_3 (ppbv), and **(c)** STEM column O_3 ($\times 10^{16}$ molecules/cm^2). Columns 1-3 show R(O_3, EAS, 20%) from the simulations associated with GEOS-Chem, ECMWF C-IFS, and RAQMS, respectively. Column 4 shows 1/5 of the R(O_3, EAS, 100%) from the simulations related to RAQMS. **(d)** The STEM/RAQMS-based "Scalability" S_{O3} (eq. (3)) of the NAM surface (left) and column (right) in June 2010.

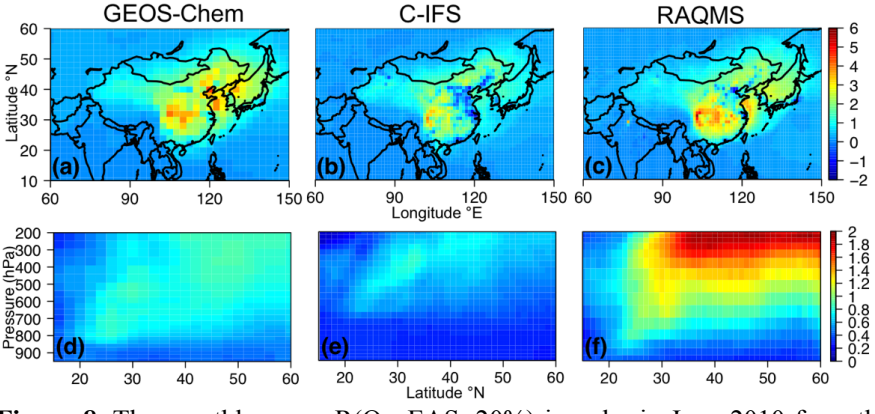

Figure 8. The monthly-mean R(O_3, EAS, 20%) in ppbv in June 2010 from the three boundary condition models at the source and near the receptor regions: **(a-c)** surface O_3 in the East Asia; and **(d)** O_x (GEOS-Chem) or **(e-f)** O_3 (ECMWF C-IFS and RAQMS) along the cross section of 135°W (near the west boundary of the STEM model domain as defined in Figure 2b).

Atmos. Chem. Phys. Discuss., doi:10.5194/acp-2016-958, 2016
Manuscript under review for journal Atmos. Chem. Phys.
Published: 28 November 2016

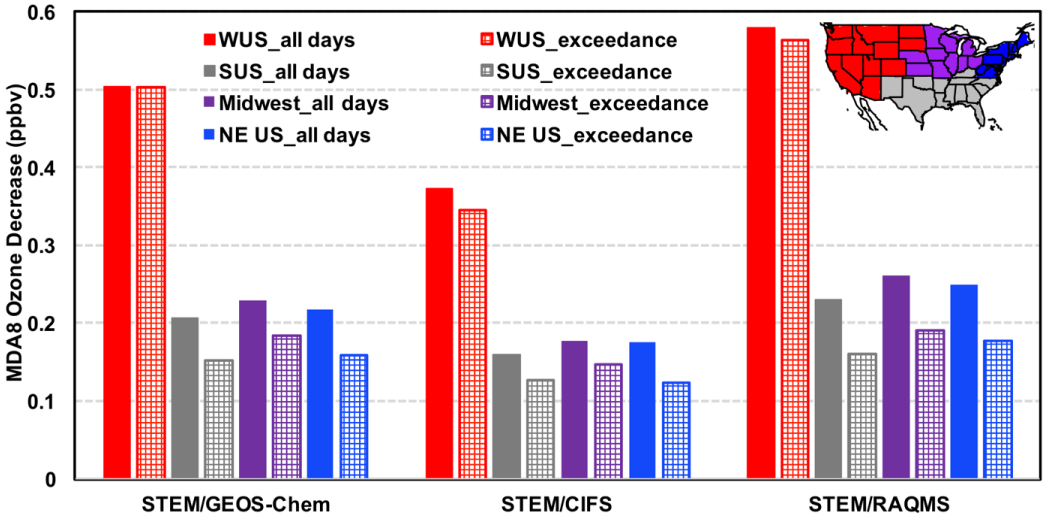

Figure 9. STEM R(MDA8, EAS, 20%) for May-June 2010 in four US subregions (defined in the inset of panel, also consistent with the definitions in Figures 2/S3 and Tables 2-3), averaged on all days (bars with solid fill) and only on the days when the simulated total MDA8 O_3 concentrations were over 70 ppbv (bars with grid pattern fill). The results from the STEM runs using GEOS-Chem, ECMWF C-IFS and RAQMS boundary conditions are shown separately.

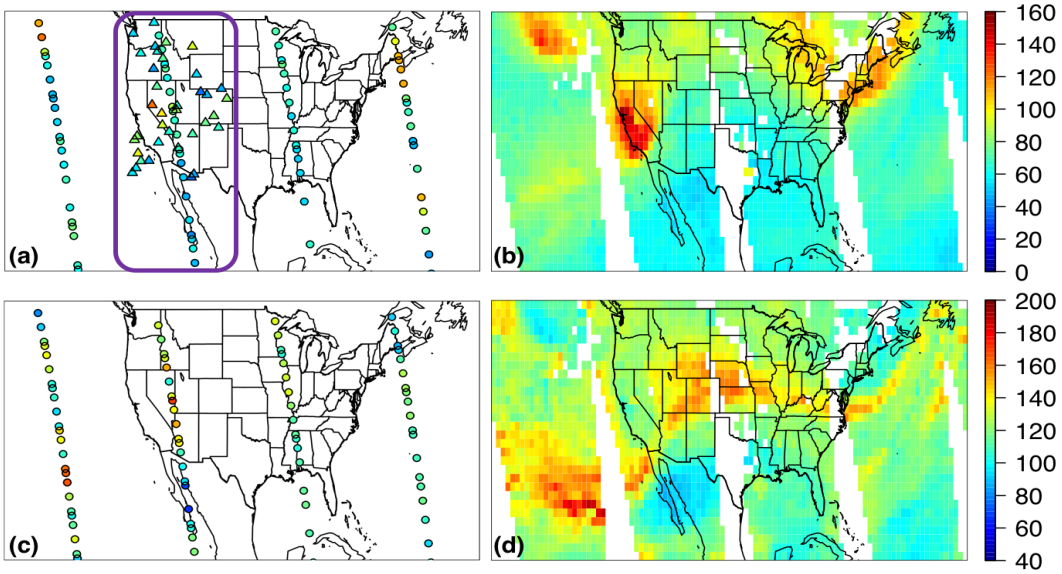

Figure 10. Case study of 9 May 2010: **(a-b)** Ozone (ppbv) and **(c-d)** CO (ppbv) at ~500 hPa from the L2 **(a;c)** TES retrievals (circles) and **(b;d)** L3 AIRS products at early afternoon local time. The L2 IASI O_3 (ppbv) at ~500 hPa retrieved using the TES algorithm (details in Section 2.3.2) at the mid- morning local times is shown on panel (b) as triangles. The O_3 profiles within the purple box in panel (a) were used in the model evaluation shown in Figure 11.

Atmos. Chem. Phys. Discuss., doi:10.5194/acp-2016-958, 2016
Manuscript under review for journal Atmos. Chem. Phys.
Published: 28 November 2016

Atmospheric Chemistry and Physics Discussions

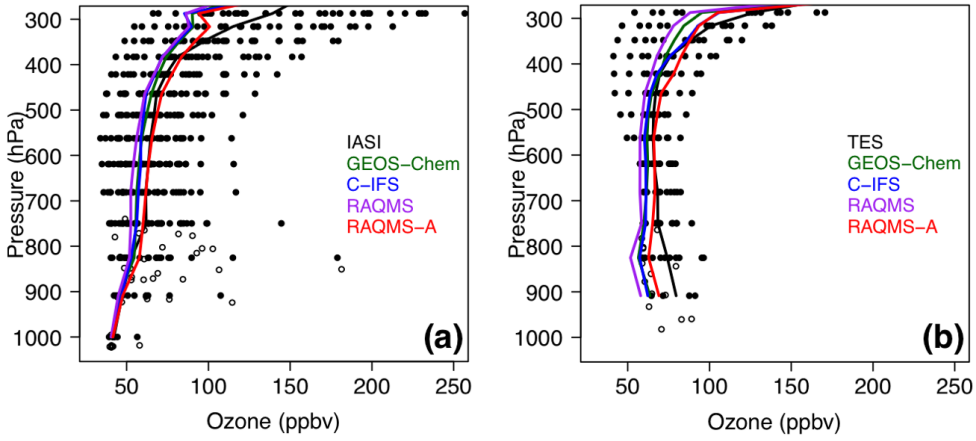

Figure 11. Case study of 9 May 2010: The comparisons between **(a)** IASI and **(b)** TES O_3 in the western US with the simulated O_3 in the STEM runs using the GEOS-Chem (green), C-IFS (blue), RAQMS (purple), and assimilated RAQMS (red) boundary conditions. The O_3 profiles within the purple box in Figure 10a were used in the evaluation. Observation operators were applied in the comparisons (details in Section 2.3.2). Solid and open dots are TES/IASI data at the TES retrieval reporting levels and at the variable surface pressure levels, respectively. Solid lines are median O_3 profiles from the satellite observations and the different STEM simulations, calculated only on the TES retrieval reporting levels.

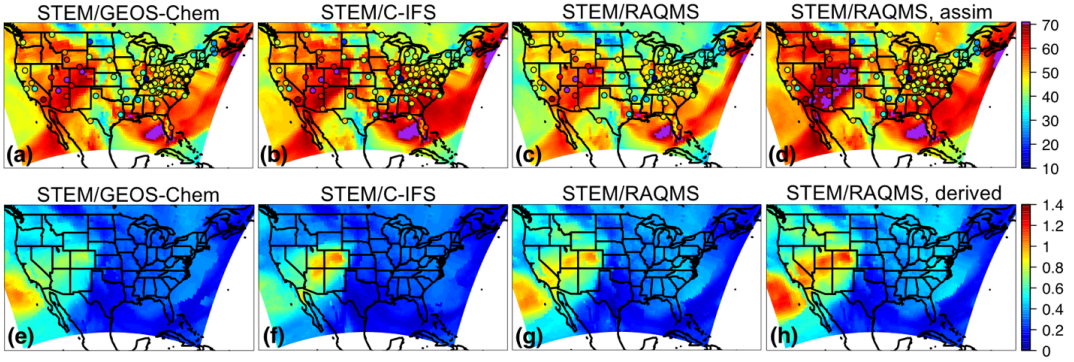

Figure 12. Case study of 9 May 2010: **(a-d)** Surface MDA8 total O_3 and **(e-h)** surface R(MDA8, EAS, 20%) from the STEM simulations using the (**a;e**) GEOS-Chem, **(b;f)** ECMWF C-IFS, and **(c;g)** RAQMS free run as the boundary conditions. **(d)** Surface MDA8 total O_3 in a STEM base simulation using the RAQMS assimilation run as the boundary conditions. CASTNET observations are overlaid in filled circles in panels (a-d). **(h)** 1/5 of the surface R(MDA8, EAS, 100%) from STEM/RAQMS simulations. The conditions at ~400-500 hPa are shown in Figure S4.

Atmos. Chem. Phys. Discuss., doi:10.5194/acp-2016-958, 2016
Manuscript under review for journal Atmos. Chem. Phys.
Published: 28 November 2016

Atmospheric Chemistry and Physics Discussions

Table 1a. HTAP2 base and sensitivity simulations by various global models. Relevant references for the RAQMS model and the SNU GEOS-Chem are Pierce et al. (2007, 2009) and Park et al. (2004) (with additional descriptions on its HTAP2 simulation configurations at: http://iek8wikis.iek.fz-juelich.de/HTAPWiki/WP2.3?action=AttachFile&do=view&target=_README_GEOS-Chem.pdf), respectively, and the descriptions of the rest six global models can be found in published HTAP2 works such as in Stjern et al. (2016). The STEM boundary condition models are highlighted in bold.

Global model and horizontal resolution	BASE	EASALL -20%	EASALL -100%	GLOALL -20%	NAMALL -20%	EURALL -20%	SASALL -20%
CAM-Chem, 2.5°×1.9°	✓	✓		✓	✓	✓	✓
CHASER T42, ~2.8°×2.8°	✓	✓		✓	✓	✓	✓
EMEP rv48, 0.5°×0.5°	✓	✓		✓	✓	✓	✓
SNU GEOS-Chem v9-01-03, 2°×2.5°	✓	✓		✓	✓		
CU-Boulder GEOS-Chem adjoint v35f, 2°×2.5°	✓	✓		✓	✓	✓	✓
RAQMS, 1°×1°, free running	✓	✓	✓				
RAQMS, 1°×1°, w/ satellite assimilation	✓						
Oslo, ~2.8°×2.8°	✓	✓		✓	✓	✓	✓
ECMWF CIFS, ~0.7°×0.7°/1.125°×1.125° (used as the STEM chemical boundary conditions)	✓	✓		✓	✓	✓	✓

Table 1b. STEM regional simulations for HTAP2

Boundary condition model	BASE	EASALL -20%	EASALL -100%
SNU GEOS-Chem v9-01-03, 2°×2.5°	✓	✓	
RAQMS, 1°×1°, free running	✓	✓	✓
RAQMS, 1°×1°, w/ satellite assimilation	✓		
ECMWF CIFS, 1.125°×1.125°	✓	✓	

Atmos. Chem. Phys. Discuss., doi:10.5194/acp-2016-958, 2016
Manuscript under review for journal Atmos. Chem. Phys.
Published: 28 November 2016

Atmospheric Chemistry and Physics Discussions

Table 2. Evaluation of the period mean (1 May-30 June, 2010) multi- global model free simulations against the CASTNET observations, only at the sites where 95% of the hourly O_3 observations are available.

Subregion	US EPA regions contained	Number of sites	Mean bias (ppbv)		RMSE (ppbv)	
			3 BC[a] models	8 global models	3 BC models	8 global models
Western US	8, 9, 10	19	-5.68	-2.52	10.37	7.05
Southern US	4, 6	18	11.61	10.24	13.62	11.96
Midwest	5, 7	13	8.03	7.66	9.16	8.67
Northeast	1, 2, 3	17	9.55	10.63	10.28	11.24
All	1-10	67	5.49	6.22	11.11	9.96

[a]BC: Boundary Conditions

Table 3. Evaluation of the hourly STEM simulated total O_3 (averaged from the three base simulations that used the different free-running boundary conditions) against the CASTNET surface observations for 8 May-30 June, 2010. The subregional mean R(O_3, EAS, 100%), as well as its correlation coefficient with the observed O_3 are also shown.

Subregion	US EPA regions contained	Number of sites	Mean elevation (km): actual/ model	Mean bias (ppbv)	RMSE (ppbv)	Correlation (model base; obs)	Correlation (obs; modeled EAS)	Mean EAS sensitivity (ppbv)
Western US	8, 9, 10	22	1.75/ 1.71	1.60	4.86	0.76	0.34	0.48
Southern US	4, 6	22	0.38/ 0.31	20.33	22.13	0.58	0.27	0.15
Midwest	5, 7	16	0.29/ 0.28	15.64	17.97	0.70	0.15	0.17
Northeast	1, 2, 3	20	0.36/ 0.26	20.94	24.16	0.47	0.17	0.21
All	1-10	80	0.73/ 0.68	16.17	18.30	0.66	0.13	0.20

Atmos. Chem. Phys. Discuss., doi:10.5194/acp-2016-958, 2016
Manuscript under review for journal Atmos. Chem. Phys.
Published: 28 November 2016

Atmospheric Chemistry and Physics Discussions

Table 4. The ranges and standard deviations (ppbv, separated by ";") of R(O_3, *source region*, 20%) by 6-8 global models (defined in eq. (1a-d)), summarized by months in 2010. The monthly multi-model mean values are shown in Figures 5-6.

Month/ Source region	All Foreign/ Non-NAM (ppbv)	EUR (ppbv)	EAS (ppbv)	SAS (ppbv)
Jan	0.38-1.69; 0.41	0.002-0.12; 0.05	0.02-0.72; 0.24	0.001-0.11; 0.04
Feb	0.92-2.07; 0.37	0.02-0.15; 0.05	0.16-0.91; 0.28	0.02-0.12; 0.04
Mar	1.30-2.37; 0.38	0.07-0.21; 0.06	0.24-1.03; 0.30	0.03-0.12; 0.03
Apr	1.42-2.46; 0.33	0.09-0.23; 0.05	0.33-1.07; 0.28	0.04-0.12; 0.03
May	1.24-1.91; 0.21	0.06-0.17; 0.04	0.24-0.75; 0.19	0.05-0.11; 0.02
Jun	1.03-1.41; 0.13	0.03-0.07; 0.02	0.14-0.39; 0.09	0.04-0.07; 0.01
Jul	0.86-1.18; 0.13	0.02-0.04; 0.01	0.08-0.22; 0.06	0.01-0.04; 0.01
Aug	0.80-1.19; 0.13	0.01-0.04; 0.01	0.07-0.20; 0.05	0.02-0.04; 0.01
Sep	0.85-1.18; 0.13	0.03-0.05; 0.01	0.10-0.25; 0.06	0.02-0.06; 0.01
Oct	0.96-1.31; 0.14	0.04-0.10; 0.02	0.17-0.42; 0.09	0.03-0.08; 0.02
Nov	0.90-1.48; 0.19	0.05-0.15; 0.04	0.17-0.54; 0.14	0.04-0.10; 0.02
Dec	0.73-1.67; 0.29	0.03-0.18; 0.05	0.14-0.66; 0.19	0.04-0.12; 0.03